Charge symmetry breaking two-pion exchange

J. A. Niskanen*
Indiana University Cyclotron Facility and Nuclear Theory Center, 2401 Milo B. Sampson Lane, Bloomington, Indiana 47405
(Received 14 February 1992)

Two-pion exchange (TPE) contribution to the charge symmetry breaking class IV neutron-proton interaction is examined in a potential and coupled channels approach. Based on nonrelativistic πNN and $\pi N\Delta$ vertices, a TPE interaction is treated in two ways, as a potential or as a part calculable by the coupled channels method plus a residual potential interaction. A practical parametrization of the TPE potentials is given, which can also be used in the case of class III charge symmetry breaking (CSB) forces as well as for charge symmetric interactions. The results show that below 300 MeV the TPE contribution to CSB in elastic *np* scattering is insignificant, whereas at higher energies it should not be neglected.

PACS number(s): 13.75.Cs, 21.30.+y, 11.30.Er

I. INTRODUCTION

One of the most widely used and successful symmetries in nuclear physics is charge independence or isospin symmetry of nuclear forces. It is obviously broken in electromagnetic interactions but is known to be broken even in the strong interaction due to electromagnetic effects within hadrons and differences of quark masses. This breaking of the isospin symmetry in the nuclear force has been studied for a long time. However, earlier research has mostly concentrated on looking for differences in the *pp* vs *np* system or in the *pp* vs *nn* interaction. In the terminology of Henley and Miller [1] these differences arise from isospin asymmetric forces of class II (isotensor) and III (proportional to the total isospin vector $\tau_{10}+\tau_{20}$). The latter is a *charge symmetry breaking* (CSB) force and it distinguishes between isospin mirror systems. For nucleons CSB means simply a way to tell the neutron from the proton in an experiment. CSB interactions of class III have been typically studied in nuclear mirror systems or comparing *pp* and *nn* low-energy scattering parameters. Both of these approaches are hampered by difficulties with nuclear structure treatment, extraction of the Coulomb interaction from the *pp* system, or the three-body nature of experiments with neutron targets.

Not until very recently has the *class IV CSB force,* which acts only in the *np* system and actually changes the isospin, become experimentally tractable. In the presence of this interaction the analyzing power (or polarization) of the proton is different from that of the neutron in *np* scattering. At present there are two data points for the difference of the proton and neutron analyzing powers $\Delta A = A_n - A_p$ in elastic *np* scattering. The TRIUMF experiment [2] at 477 MeV gave $\Delta A(72°) = 0.0047 \pm 0.0022 \pm 0.0008$ and the preliminary angle averaged Indiana University Cyclotron Facility (IUCF) result at 183 MeV is [3] $\Delta A(82°-116°) = 0.003\,31 \pm 0.000\,59 \pm 0.000\,43$. Unfortunately it appears impossible to extend these already difficult experiments outside the neighborhood of the angle where A_n or A_p crosses through zero and obtain a full angular distribution of ΔA, although the IUCF experiment can give some features of it. Measurements are possible at this particular angle, since many systematic error sources cancel off there. For example, the TRIUMF experiment measured directly the difference in the zero crossing angles of A_p and A_n rather than A's themselves, so that the knowledge of the absolute normalization of the polarization was not so crucial. Knowing the slope of the analyzing power $A(\theta)$ one can then deduce ΔA at this angle with first-order uncertainties in the beam and target polarization vanishing. The IUCF measurement, on the other hand, is based on the assumptions of the constancy of the uncertainty of $A(\theta)$ around the zero crossing angle, in which case the measured apparent difference is

$$\Delta A(\theta) = \Delta A_{\text{true}}(\theta) + \text{const} \times A(\theta) \ . \tag{1}$$

In an average about the zero crossing angle the latter term carrying the dominant uncertainty about the absolute polarization cancels off. Another experimental proposal at TRIUMF suggests to measure ΔA at the energy 350 MeV, intermediate between the present data [4].

There has been a considerable amount of theoretical activity to predict or reproduce these numbers [5–10] (for up-to-date overviews see Refs. [11] and [12]). Most theoretical calculations are able to explain the meager data by meson exchanges. The TRIUMF result originates nearly totally from the mundane one-pion exchange if the neutron-proton mass difference is taken into account, because other effects are small at the zero crossing angle at 477 MeV. The IUCF number, on the other hand, consists of nearly equal contributions from one-pion exchange (OPE), the magnetic interaction of the neutron dipole moment with the proton charge and the more interesting short-ranged $\rho\omega$ mixing in heavy meson exchange. The comparable significance of the last mechanism makes the lower-energy measurement of IUCF im-

*On leave from Department of Theoretical Physics, University of Helsinki, Siltavuorenpenger 20 C, SF-00170 Helsinki, Finland.

portant in studies of the short-range behavior of the strong interaction. Figures 1 and 2 show the two existing data points together with theoretical predictions of Ref. [8]. The difference between the dashed and dash-dotted curves is due to heavy mesons, mainly $\rho\omega$ mixing.

The class IV CSB potential responsible for ΔA in np scattering can be of two spin and isospin changing forms

$$V_{\mathrm{IVa}}=(\tau_1\times\tau_2)_0\sigma_1\times\sigma_2\cdot\mathbf{L}v(r)\ , \tag{2a}$$

$$V_{\mathrm{IVb}}=(\tau_1-\tau_2)_0(\sigma_1-\sigma_2)\cdot\mathbf{L}v(r)\ . \tag{2b}$$

Quite obviously the former of these interactions arises only in exchanges of a *charged* particle (or effective particle). By far, the dominant contribution here is the effect of the np mass difference in the charged pion vertex. In contrast, the latter is due to *neutral* exchanges, most typically the magnetic interaction between the neutron and proton or $\rho\omega$ meson mixing. The two forms of CSB force give rise to qualitatively different angular distributions of $\Delta A(\theta)$, the latter being rather similar to $A_p(\theta)$ or $A_n(\theta)$ for intermediate energies and consequently small at the zero crossing angle of these observables. A possible qualitative reason for this similarity may be the structural likeness of the potential V_{IVb} to the spin-orbit force (which, of course, conserves the spin and isospin). Because for a given total angular momentum J the dominant mixed states have both either an attractive or repulsive phase (i.e., the triplet and singlet are similar), also the spin mixing transition matrix is similar in phase to that due to the spin-orbit force in these tensor uncoupled partial waves. The tensor coupled states have much smaller phases and may be less important in the analyzing power and polarization. The interaction V_{IVa}, in contrast, has an additional state-dependent phase $(-1)^J$, which removes the chance of any resemblance of $\Delta A(\theta)$ to $A(\theta)$. Thus the partial wave mixing parameters for IVb are uniformly of the same sign (for the important $\rho\omega$ mixing and the magnetic positive), while those for IVa (OPE) alternate their sign with J. This qualitative difference is clearly seen in Figs. 1 and 2, with neutral

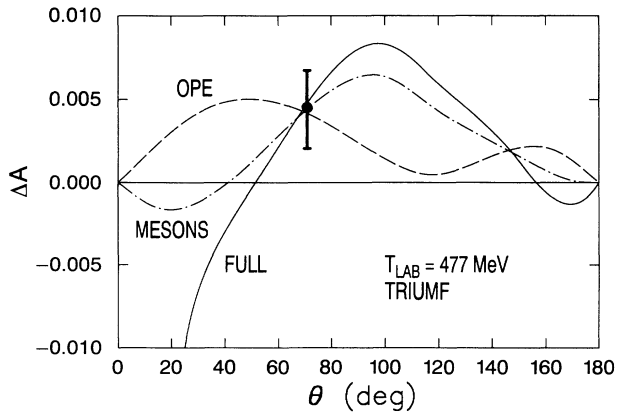

FIG. 1. The experimental data point of TRIUMF [2] at 477 MeV vs theoretical results of Ref. [8]. OPE with the np mass difference (dashed curve), including also heavier mesons (mainly $\rho\omega$ meson mixing, dash-dotted), including also the interaction of the neutron magnetic moment with the proton charge (solid).

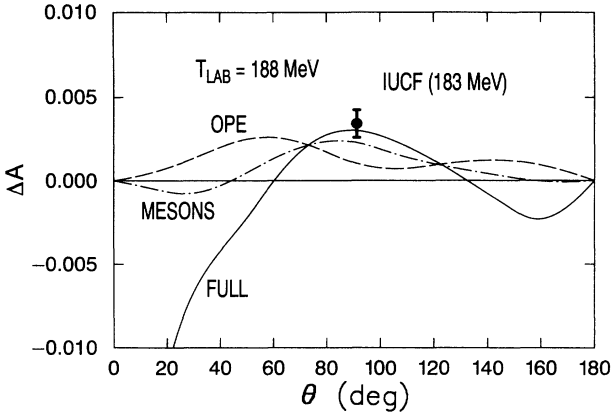

FIG. 2. As Fig. 1 but theory at 188 MeV, experiment at 183 MeV [3].

particle exchange contributions also changing their signs near the zero crossing angle, whereas OPE is positive with a principal and secondary maximum in the forward and backward directions.

Since the interactions (2) change the spin and isospin, triplet and singlet states of a given $L=J$ are mixed. This mixing can be expressed as an S-matrix parametrization

$$S=\begin{bmatrix} \cos2\gamma_J e^{2i\bar{\delta}_J} & i\sin2\gamma_J e^{i(\bar{\delta}_J+\bar{\delta}_{JJ})} \\ i\sin2\gamma_J e^{i(\bar{\delta}_J+\bar{\delta}_{JJ})} & \cos2\gamma_J e^{2i\bar{\delta}_{JJ}} \end{bmatrix}\ , \tag{3}$$

where γ_J is the mixing parameter analogous to $\bar{\epsilon}_J$, and $\bar{\delta}_J$ ($\bar{\delta}_{JJ}$) is the two nucleon "bar" phase shift for the particular singlet (triplet) state in question. At low and intermediate energies the $^3P_1$-$^1P_1$ and $^3D_2$-$^1D_2$ mixings are dominant. The relation of these partial wave mixing parameters to the isospin breaking angle-dependent spin amplitude $f(\theta)$ and the observable $\Delta A(\theta)$ can be found in earlier calculations of CSB [6,8] or the compilation [14] of spin $\frac{1}{2}+\frac{1}{2}$ scattering observables.

One reason for the recent interest in isospin breaking, especially charge symmetry breaking, is the hope that its detailed understanding could tell something about the underlying hadron structure in terms of quarks or solitons etc. In principle, one might be able to gain information about the strong interaction, which is complementary to the isospin symmetric case. In particular, the meson exchange model of nuclear forces can be *tested in a new environment where it was not originally fitted.* At the very least new constraints on, e.g., meson-nucleon couplings could be expected, since meson exchanges appear in different combinations as compared with the isospin conserving case [8]. On the other hand, deviations from the meson exchange picture could be signatures of a deeper mechanism.

A particularly interesting candidate for such a "smoking gun effect" of quarks in intermediate energy physics is the spectacularly great theoretical difference between the short-range $\rho\omega$ mixing effect and CSB quark-gluon calculations [13]. All meson exchange calculations give relatively strong charge symmetry violation arising from $\rho\omega$ mixing, whereas the quark-gluon result is totally

negligible. One might note the difference to the situation in the case of isospin respecting nuclear force, where the quark-gluon exchange mechanisms give results which are similar to vector meson exchanges. Therefore, at the one σ confidence level the IUCF result would appear to lend some support to the meson exchange model of the NN interaction even at short distances. However, before jumping to hasty conclusions of any exotic or quark effects vs heavy meson exchanges at intermediate energies in interpreting any experiments, careful calculations are needed also at the hadron level. The aim of this paper is to fill a void concerning relatively long-ranged two meson exchange effects, on which rather little work has been done in the case of class IV forces. Because, as will be seen later in Sec. II B, even the charge-independent two-pion exchange (TPE) looks partly like a vector meson exchange, it could well give also CSB contributions similar to $\rho\omega$ meson mixing. Furthermore, scalar meson exchange with the np mass difference included gives rise to a CSB effect very similar to what $\rho\omega$ mixing does [8]. Since much of TPE is often simulated by a significant σ meson exchange in meson theoretical potentials, it is essential to get estimates of CSB in two meson exchange. However, it was seen in Ref. [8] that the σ exchange is a small effect, partly because of the above qualitative similarity of the angular dependence to $A(\theta)$. On the other hand, in TPE charged mesons can be exchanged resulting in a class IVa interaction, which may be important at the crossover angle.

Charge-dependent TPE interactions have been studied very little earlier applying the Partovi-Lomon formalism [15] in the case of class IV forces [6] and in the case of classes II and III [16]. However, these works considered only nucleonic states, no baryon internal excitations, in particular Δ, are included, except in the study of isotensor forces of Ref. [17]. These are known to be very important in $T=1$ scattering. Perturbation approach to isobar effects may be questionable. Although CSB itself is weak, the CSB $N\Delta$ states (originating from $T=0$ initial NN states) are coupled strongly to $T=1$ NN states. The $N\Delta$ components should be generated as exactly as possible from $T=1$ states and then be coupled by a weaker CSB potential to $T=0$ states. That is to say, the DWBA starting point should be a distorted wave function including $N\Delta$ admixtures as exactly as possible. The coupled channels technique is a very good practical method to achieve these. Although, in principle, DWBA would then be quite adequate to calculate CSB, it is just as easy to consider the $T=0$ NN state as still another coupled channel and solve the whole system exactly.

The outline of this paper is as follows. First in Sec. II the CSB OPE is briefly presented both with the CSB πNN vertex (including the np mass difference) and with the CSB $\pi N\Delta$ vertex. Then the two meson exchange contribution is introduced for the isospin symmetric and CSB case along with a practical technical division to coupled channels plus a potential. Both NN and $N\Delta$ intermediate states are considered including both box and crossed box diagrams. The results of the numerical calculations are given in Sec. III.

II. THEORY

A. CSB in one-pion exchange

The primary origin of charge symmetry breaking considered in this work is the neutron-proton mass difference in the pion-nucleon coupling or the corresponding mechanism in the $\pi N\Delta$ vertex. It has been known for a long time that the CSB structure of the πNN coupling is in the nonrelativistic limit

$$\begin{aligned} H_{\pi NN} &= H_0 + H_1 + H_2 \\ &= -i\frac{f}{\mu}[(\mathbf{p}'-\mathbf{p})\cdot\boldsymbol{\sigma}\boldsymbol{\tau}\cdot\boldsymbol{\phi} + (\mathbf{p}'-\mathbf{p})\cdot\boldsymbol{\sigma}\phi_0\delta \\ &\quad + i(\mathbf{p}'+\mathbf{p})\cdot\boldsymbol{\sigma}(\boldsymbol{\tau}\times\boldsymbol{\phi})_0\delta] \ . \end{aligned} \tag{4}$$

Here $\mathbf{p}$ and $\mathbf{p}'$ are the initial and final nucleon momenta and $\boldsymbol{\sigma}$ and $\boldsymbol{\tau}$ are the spin and isospin operators. The pion field is $\boldsymbol{\phi}$ and its mass μ. The small parameter of the theory is

$$\delta = \frac{M_n - M_p}{M_n + M_p} \ , \tag{5}$$

and only terms in the zeroth or first order have been kept in Eq. (4). The pion-nucleon coupling constant is given by $f^2/4\pi = 0.075$ [18]. This coupling is in good accord with the one used in the Reid potential [19], which will be used as the basis of strong interaction distortions. Although over the recent years evidence has accumulated for the favor of this value, it is not yet completely without controversy [41]. Also in comparisons with earlier calculations it might be useful to use the older larger coupling 0.079. The two-pion exchange CSB results presented in this paper scale simply as f^4 in the case of nucleonic intermediate states and as f^2 in the case of isobar excitation. In the coordinate space the above pion-nucleon vertex can also be presented as

$$H = -\frac{f}{\mu}\boldsymbol{\sigma}\cdot\{\nabla\boldsymbol{\tau}\cdot\boldsymbol{\phi}(\mathbf{x}) + \delta\nabla\phi_0(\mathbf{x}) + \delta(\mathbf{p}+\mathbf{p}')[\boldsymbol{\tau}\times\boldsymbol{\phi}(\mathbf{x})]_0\} \ . \tag{6}$$

The pion-nucleon coupling (4) leads to the one-pion exchange interaction

$$V(\mathrm{OPE}) = \frac{f^2}{4\pi}\frac{1}{\mu^2}\left[\nabla\cdot\boldsymbol{\sigma}_1\nabla\cdot\boldsymbol{\sigma}_2\left[\frac{e^{-\mu r}}{r}\right][\boldsymbol{\tau}_1\cdot\boldsymbol{\tau}_2 + (\boldsymbol{\tau}_1+\boldsymbol{\tau}_2)_0\delta] - 2\delta(\boldsymbol{\tau}_1\times\boldsymbol{\tau}_2)_0\boldsymbol{\sigma}_1\times\boldsymbol{\sigma}_2\cdot\mathbf{L}\frac{1}{r}\frac{d}{dr}\left[\frac{e^{-\mu r}}{r}\right]\right] \ . \tag{7}$$

In practice, of course, some form factor is also included in the vertices and the potential. It is clear from Eq. (7) that in OPE the *np* mass difference effect leads into a class III CSB force in the case of neutral pion exchange, whereas the exchange of charged pions gives a class IVa interaction. This potential is able to explain most of the ΔA observed in the TRIUMF experiment of Ref. [2] at the angle where A goes through zero. However, other possible contributions should be carefully evaluated to have a meaningful comparison with the data. Caution is especially important for the interpretation of the IUCF result of Ref. [3], where also other effects are significant.

If the CSB πNN vertex is considered to originate at the quark level from the differences of the constituent quark masses, it is easy to show in the nonrelativistic quark model that also $\pi N\Delta$ coupling has a similar isospin dependence [20]

$$H_{\pi N\Delta}=H_0'+H_2' =-i\frac{f^*}{\mu}[(\mathbf{p}'-\mathbf{p})\cdot\mathbf{S}\mathbf{T}\cdot\boldsymbol{\phi}+i(\mathbf{p}'+\mathbf{p})\cdot\mathbf{S}(\mathbf{T}\times\boldsymbol{\phi})_0\delta] . \tag{8}$$

As a difference to the πNN case, now **S** and **T** are the transition spin and isospin operators for $N\to\Delta$ and the coupling constant is $f^{*2}/4\pi=0.35$ from the free Δ width [21]. Another difference is that the term H_1' analogous to H_1 of Eq. (4) is missing, since the transition necessarily needs an isospin operator. The second term is similar to H_2 of Eq. (4) and will give rise to a CSB transition potential like the last term in Eq. (7). The simple quark arguments would give for the splitting of the successive charge states of the Δ the same 1.3 MeV as for the nucleons. This agrees very well with the known mass relations [22]

$$\Delta^0-\Delta^{++}=2.7\pm0.3\ \text{MeV} , \qquad \Delta^--\Delta^{++}+\frac{\Delta^0-\Delta^+}{3}=4.6\pm0.2\ \text{MeV} . \tag{9}$$

Similarly to the OPE potential between nucleons one gets a transition potential for $NN\leftrightarrow\Delta N+N\Delta$ as

$$V_{\rm tr}(\text{OPE})=\frac{ff^*}{4\pi}\frac{1}{\mu^2}\left[\nabla\cdot\mathbf{S}_1\nabla\cdot\boldsymbol{\sigma}_2\left[\frac{e^{-\mu r}}{r}\right](\mathbf{T}_1\cdot\boldsymbol{\tau}_2+T_{10}\delta)-2\delta(\mathbf{T}_1\times\boldsymbol{\tau}_2)_0\mathbf{S}_1\times\boldsymbol{\sigma}_2\cdot\mathbf{L}\frac{1}{r}\frac{d}{dr}\left[\frac{e^{-\mu r}}{r}\right]+(1\leftrightarrow2)\right] . \tag{10}$$

The CSB term proportional to T_{10} arises only from CSB in the nucleon end of the pion exchange. The first term conserves the isospin and is nonzero only for $T=1$ nucleon states, whereas either of the CSB terms can cause a transition from an initial $T=0$ state. Finally another iteration of $V_{\rm tr}$ brings the system back to a $T=1$ NN state, causing a net isospin breaking in the two nucleon system.

This transition potential approach to CSB has so far been applied by the coupled channels method to incorporate box diagrams with Δ's in Refs. [20,23,24]. Reference [24] showed that below, say, 500 MeV the effect of inelasticities closely related to the Δ are small but at higher energies they become non-negligible. That work was not a totally systematic treatise of the Δ effects in that, for example, the crossed box diagrams were not considered. We shall now proceed to introduce CSB two meson mechanisms in a more systematic way and then consider a hybrid approach by treating a box part with the more exact coupled channels method and the remainder as a two meson exchange potential.

B. Isospin conserving two-pion exchange

In deriving the box and crossed box diagram contributions as meson exchange interaction the kinematics will be fixed as easy and symmetric as possible and is shown in Fig. 3. In these diagrams an overall momentum **q** is transferred to the particle 1 and the average relative momentum of the nucleons is **p**. The momentum **k** is a loop integral variable. Also the formalism is kept nonrelativistic (except for kinematics) with no attention to the relativistic off-shell behavior of the Δ propagator [25].

To the extent that the angular dependence of the propagators can be omitted in the integration over **k**, the space-spin and isospin structure obtained from the isospin symmetric vertices is

$$\text{box}=\left[\frac{ff^*}{\mu^2}\right]^2\left[\frac{2}{3}(k^2-q^2/4)^2+\frac{1}{27}q^2k^2(2\boldsymbol{\sigma}_1\cdot\boldsymbol{\sigma}_2-S_{12})\right](2+\tfrac{2}{3}\boldsymbol{\tau}_1\cdot\boldsymbol{\tau}_2) ,$$
$$\text{crossed}=\left[\frac{ff^*}{\mu^2}\right]^2\left[\frac{2}{3}(k^2-q^2/4)^2-\frac{1}{27}q^2k^2(2\boldsymbol{\sigma}_1\cdot\boldsymbol{\sigma}_2-S_{12})\right](2-\tfrac{2}{3}\boldsymbol{\tau}_1\cdot\boldsymbol{\tau}_2) , \tag{11}$$

where the tensor operator is defined as

$$S_{12}=3\boldsymbol{\sigma}_1\cdot\hat{\mathbf{q}}\boldsymbol{\sigma}_2\cdot\hat{\mathbf{q}}-\boldsymbol{\sigma}_1\cdot\boldsymbol{\sigma}_2 . \tag{12}$$

The omission of odd powers in **k** is justified, if the energy denominators are even with respect to the direction of **k**. This is true for all but the kinetic energies of the intermediate baryons in the box diagrams. The pion energies do not give odd **k** dependence, since all vectors $\mathbf{k}-\mathbf{q}/2$

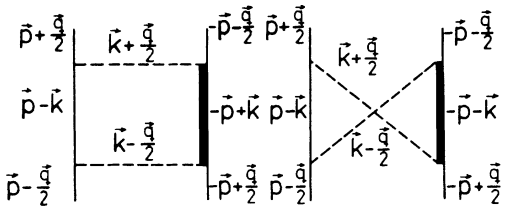

FIG. 3. The choice of momenta for calculating two-pion exchange contributions. The overall momentum transfer is $\mathbf{q}$ and $\mathbf{k}$ is an integration variable.

appear with a corresponding $\mathbf{k}+\mathbf{q}/2$, and in a sum over diagrams the pair combines to an even function of $\cos\theta_{kq}$. It is easy to infer from Fig. 3 that only in the box diagrams does $\cos\theta_{kp}$ survive unpaired in odd powers. In the limit of static baryons this dependence vanishes as a relativistic correction. Its effect will be studied to some extent later. Of course, the survival of an "odd" $\mathbf{k}$ in the numerator has nothing to do with parity violation, which is a weak interaction phenomenon. The momentum $\mathbf{k}$ is always combined with another vector and parity is conserved. The pion energies can contribute via $\cos^2\theta_{kq}$ or higher even powers to the quadratic spin-orbit and other terms. The "small" parameter of this expansion would be $k^2q^2\cos^2\theta_{kq}/(\mu^2+k^2+q^2/4)^2<1$ and its effect to the numerator will be omitted. However, in the following discussions, when the propagators themselves are calculated, the angular dependence on θ_{kq} will be included. The factor 4π arising from the angular integration will be included in the propagators.

The above differences between the box and crossed box diagram contributions are, of course, due to the commutation rules of the spin and isospin operators in the exchange of the pion absorption and creation operators on, say, nucleon 2. They do not depend on other time orderings as long as the property box or crossed is fixed. The operator is directly symmetric in the exchange of $1\leftrightarrow 2$ so that the excitation of each nucleon will simply be an overall multiplicative factor 2. It is interesting to note that the second (spin-dependent) term inside the brackets is exactly of the form obtained nonrelativistically for vector meson exchange with the meson nucleon coupling of the form $\boldsymbol{\sigma}\times\mathbf{q}\cdot\mathbf{V}$.

It can immediately be seen that, if the propagators for the two classes were the same, the terms with odd number of spin or isospin operators would cancel leaving only the terms scalar isoscalar and vector isovector. The former of these is the basis of simulating the isobar effect by a scalar meson σ. Of course, the simulation does not take into account the energy dependence in any way and even this simple OBE argument should be supplemented by an effective ρ exchange, too. However, the vector-isovector part is suppressed by a numerical factor of $\frac{1}{54}$ as compared with the scalar-isoscalar term. Furthermore, the propagators are not the same, but as seen later one may still argue that the vector-isoscalar or scalar-isovector parts should be small in comparison with the main term.

If the intermediate state is NN instead of $N\Delta$, then the corresponding contributions would be simply

$$\text{box}=\left[\frac{f}{\mu}\right]^4\left[\left[k^2-\frac{q^2}{4}\right]^2-\frac{1}{9}(2\boldsymbol{\sigma}_1\cdot\boldsymbol{\sigma}_2-S_{12})q^2k^2\right](3-2\boldsymbol{\tau}_1\cdot\boldsymbol{\tau}_2)\,,$$
$$\text{crossed}=\left[\frac{f}{\mu}\right]^4\left[\left[k^2-\frac{q^2}{4}\right]^2+\frac{1}{9}(2\boldsymbol{\sigma}_1\cdot\boldsymbol{\sigma}_2-S_{12})q^2k^2\right](3+2\boldsymbol{\tau}_1\cdot\boldsymbol{\tau}_2)\,. \tag{13}$$

The iterated OPE (box) is particularly strong in the isospin zero states and is, in fact, an important part in the deuteron binding.

Of course, the NN box contribution is included for the most part in the solution of Schrödinger equation by iteration of OPE. Even the $N\Delta$ box can be obtained in this way by the coupled channels approach. Now, since the numerator and denominator (propagator) is different for the box and crossed diagrams, one could make a separation

$$N_BD_B+N_CD_C=N_B(D_B+D_C)-(N_B-N_C)D_C\,. \tag{14}$$

The numerator N_B contains the spin-isospin structure of the box diagrams shown in the above equations, i.e., the iterated transition potential, and N_C the structure of the crossed ones. The first term on the right-hand side includes also the sum of all propagators of different time orderings (Fig. 4), which turns out to be just the propagator expected from iterating the normal OPE transition potential with an intermediate two baryon state, i.e., the same as could be obtained by a coupled channels calculation. Keeping only the box diagram propagators would *not* give this simple result but rather a transition potential with a modified range [26]. The energy denominators D will be discussed in detail later. For strong interactions the initial state can be so distorted by the intermediate

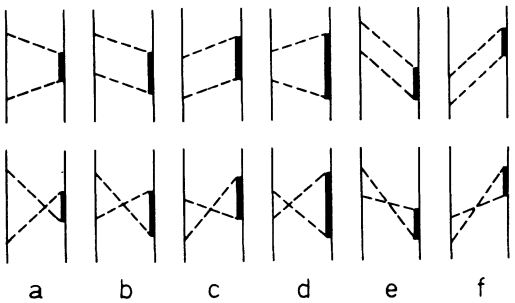

FIG. 4. Different possible time orderings of two-pion exchange.

isobar configurations that a simple iteration in second order may not be reliable but an actual coupled channels calculation would be necessary, which removes some probability from the NN state into the ΔN components. Also the relatively strong energy dependence of the box contribution especially in the $N\Delta$ threshold region is naturally treated by coupled channels. The second term on the right-hand side of Eq. (14) is then a correction that can hopefully be treated perturbatively or as an energy independent potential in the NN channel with sufficient accuracy. With $|D_C| < |D_B + D_C|$ this expectation may well be justified, but needs a numerical verification.

The above separation—keeping the box structure explicit—is suited for a separation into a coupled channels calculation plus a perturbation. A more symmetric choice for potential approaches would be

$$N_B D_B + N_C D_C = \frac{N_B + N_C}{2}(D_B + D_C) + \frac{N_B - N_C}{2}(D_B - D_C) . \tag{15}$$

The second term should be small as a difference of the propagators, whereas the first term consists only of an effective scalar-isoscalar exchange potential supplemented by a weaker vector-isovector exchange. This form justifies the expectation above that, overall, the odd spin-isospin operator terms give only a minor contribution.

C. Isospin breaking two-pion exchange

The above ideas presented for the isospin symmetric interaction can also be applied in the isospin breaking case. The two meson exchange mechanism will be separated into a part that can be treated by coupled channels plus a correction. One can have a numerical consistency check on the method by calculating the first term both as a potential and using coupled channels.

1. H_2 and H_2' vertex

Table I shows the isospin factors for each diagram in Figs. 5 and 6. The result is given both as an operator and as the matrix element for the transition from the $T=0$ state to $T=1$. One may note some symmetries such as exchanging the particles 1 and 2 (change of sign) or changing the position of the CSB vertex [here only of the type of H_2 or H_2' given in Eqs. (4) and (8)] in the otherwise similar diagrams. The change from the box to the crossed one is now much less trivial than in the isospin symmetry obeying case Sec. II B. It should be noted that the operators corresponding to individual diagrams are not time reversal invariant, although their sum is. The value of the matrix element is zero for the last four diagrams 5(e)–5(h) as it should, since the ΔN state cannot mix with the initial $T=0$ state without isospin breaking. If the initial and final states are reversed, the zeros would appear for diagrams 5(a)–5(d). At this stage it may be useful to remind that the basic isospin matrix elements are

$$\langle 10|\tau_{10}|00\rangle = 1 = \langle 00|\tau_{10}|10\rangle ,$$
$$\langle 10|\tau_{20}|00\rangle = -1 = \langle 00|\tau_{20}|10\rangle , \tag{16}$$
$$\langle 10|(\tau_1\times\tau_2)_0|00\rangle = -2i = -\langle 00|(\tau_1\times\tau_2)_0|10\rangle .$$

The space spin structure is somewhat lengthier but also straightforward to obtain. Considering only numerators arising from the vertices of Eqs. (4) and (8) and omitting odd powers of the intermediate momentum $\mathbf{k}$, as discussed in the previous subsection, we get the results given in Table II for the CSB vertices H_2 and H_2'. In Table II a shorthand notation

$$A^{\pm} = \tfrac{2}{3}(k^2 - q^2/4)(k^2 + q^2/4 \pm \mathbf{q}\cdot\mathbf{p}) ,$$
$$B = (i/3)(k^2 - q^2/4) ,$$
$$C = \tfrac{2}{9} i k^2 , \tag{17}$$
$$D = \tfrac{2}{9} k^2$$

has been used.

Combining Tables I and II and adding the strength coefficients of Eqs. (4) and (8) one obtains for the total box contribution of the type H_2 and H_2' CSB vertices as

TABLE I. The isospin factors $\tau_1\cdot\sigma\tau_1\cdot\phi\mathbf{T}_2^{\dagger}\cdot\phi(\mathbf{T}_2\times\phi)_0$ etc. for the type H_2 or H_2' of Eqs. (4) and (8) CSB vertex in two-pion exchange.

Diagram	Operator	$\langle 10\|Op\|00\rangle$
5(a)	$\frac{2}{3}i\tau_{20}+\frac{4}{3}i\tau_{10}-\frac{1}{3}(\tau_1\times\tau_2)_0$	$\frac{4}{3}i$
5(b)	$-\frac{2}{3}i\tau_{20}-\frac{4}{3}i\tau_{10}+\frac{1}{3}(\tau_1\times\tau_2)_0$	$-\frac{4}{3}i$
5(c)	$\frac{4}{3}i\tau_{20}+\frac{2}{3}i\tau_{10}+\frac{1}{3}(\tau_1\times\tau_2)_0$	$-\frac{4}{3}i$
5(d)	$-\frac{4}{3}i\tau_{20}-\frac{2}{3}i\tau_{10}-\frac{1}{3}(\tau_1\times\tau_2)_0$	$\frac{4}{3}i$
5(e)	$-\frac{2}{3}i\tau_{20}-\frac{4}{3}i\tau_{10}-\frac{1}{3}(\tau_1\times\tau_2)_0$	0
5(f)	$\frac{2}{3}i\tau_{20}+\frac{4}{3}i\tau_{10}+\frac{1}{3}(\tau_1\times\tau_2)_0$	0
5(g)	$-\frac{4}{3}i\tau_{20}-\frac{2}{3}i\tau_{10}+\frac{1}{3}(\tau_1\times\tau_2)_0$	0
5(h)	$\frac{4}{3}i\tau_{20}+\frac{2}{3}i\tau_{10}-\frac{1}{3}(\tau_1\times\tau_2)_0$	0
6(a)	$\frac{2}{3}i\tau_{20}-\frac{4}{3}i\tau_{10}+\frac{1}{3}(\tau_1\times\tau_2)_0$	$-\frac{8}{3}i$
6(b)	$\frac{2}{3}i\tau_{20}-\frac{4}{3}i\tau_{10}-\frac{1}{3}(\tau_1\times\tau_2)_0$	$-\frac{4}{3}i$
6(c)	$-\frac{4}{3}i\tau_{20}+\frac{2}{3}i\tau_{10}-\frac{1}{3}(\tau_1\times\tau_2)_0$	$\frac{8}{3}i$
6(d)	$-\frac{4}{3}i\tau_{20}+\frac{2}{3}i\tau_{10}+\frac{1}{3}(\tau_1\times\tau_2)_0$	$\frac{4}{3}i$
6(e)	$-\frac{2}{3}i\tau_{20}+\frac{4}{3}i\tau_{10}+\frac{1}{3}(\tau_1\times\tau_2)_0$	$\frac{4}{3}i$
6(f)	$-\frac{2}{3}i\tau_{20}+\frac{4}{3}i\tau_{10}-\frac{1}{3}(\tau_1\times\tau_2)_0$	$\frac{8}{3}i$
6(g)	$\frac{4}{3}i\tau_{20}-\frac{2}{3}i\tau_{10}-\frac{1}{3}(\tau_1\times\tau_2)_0$	$-\frac{4}{3}i$
6(h)	$\frac{4}{3}i\tau_{20}-\frac{2}{3}i\tau_{10}+\frac{1}{3}(\tau_1\times\tau_2)_0$	$-\frac{8}{3}i$

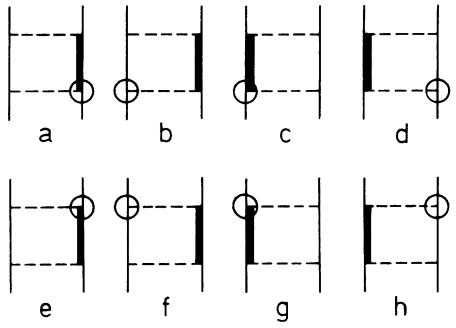

FIG. 5. CSB pion-nucleon coupling (circle) in the TPE box diagrams. Each diagram gives a different contribution to the spin-isospin structure of the numerators.

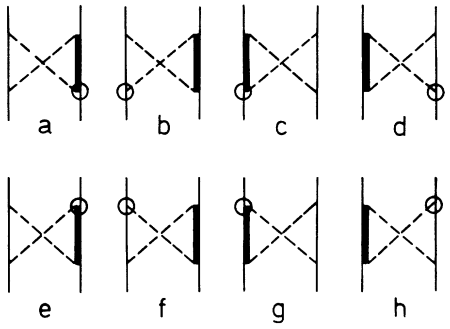

FIG. 6. CSB pion-nucleon coupling (circle) in the crossed pion diagrams.

$$\begin{aligned}\text{box}=&\left[\frac{ff^*}{\mu^2}\right]^2\frac{i\delta}{3}\{[20(C-B)i\tau_{10}+16(C-B)i\tau_{20}]\mathbf{q}\times\mathbf{p}\cdot\boldsymbol{\sigma}_1\\&+[16(C-B)i\tau_{10}+20(C-B)i\tau_{20}]\mathbf{q}\times\mathbf{p}\cdot\boldsymbol{\sigma}_2+4D(\mathbf{q}\times\mathbf{p})\cdot(\boldsymbol{\sigma}_1\times\boldsymbol{\sigma}_2)(\boldsymbol{\tau}_1\times\boldsymbol{\tau}_2)_0\}\\=&\left[\frac{ff^*}{\mu^2}\right]^2\frac{\delta}{3}\left[6\left[\frac{k^2}{3}-\frac{q^2}{4}\right]i\mathbf{q}\times\mathbf{p}\cdot(\boldsymbol{\sigma}_1+\boldsymbol{\sigma}_2)(\tau_{10}+\tau_{20})\right.\\&\left.+\frac{2}{3}\left[\frac{k^2}{3}-\frac{q^2}{4}\right]i\mathbf{q}\times\mathbf{p}\cdot(\boldsymbol{\sigma}_1-\boldsymbol{\sigma}_2)(\tau_{10}-\tau_{20})+\frac{8}{9}k^2(i\mathbf{q}\times\mathbf{p})\cdot(\boldsymbol{\sigma}_1\times\boldsymbol{\sigma}_2)(\boldsymbol{\tau}_1\times\boldsymbol{\tau}_2)_0\right]\end{aligned}\tag{18}$$

and for the crossed diagrams

$$\begin{aligned}\text{cross}=&\left[\frac{ff^*}{\mu^2}\right]^2\frac{i\delta}{3}\{4(A^-+A^+)(i\tau_{10}+i\tau_{20})+[20(C-B)i\tau_{10}-16(C-B)i\tau_{20}]\mathbf{q}\times\mathbf{p}\cdot\boldsymbol{\sigma}_1\\&+[-16(C-B)i\tau_{10}+20(C-B)i\tau_{20}]\mathbf{q}\times\mathbf{p}\cdot\boldsymbol{\sigma}_2+4D(\mathbf{q}\times\mathbf{p})\cdot(\boldsymbol{\sigma}_1\times\boldsymbol{\sigma}_2)(\boldsymbol{\tau}_1\times\boldsymbol{\tau}_2)_0\}\\=&\left[\frac{ff^*}{\mu^2}\right]^2\frac{\delta}{3}\left[-\frac{1}{3}(16k^4-q^4)(\tau_{10}+\tau_{20})+\frac{2}{3}\left[\frac{k^2}{3}-\frac{q^2}{4}\right]i\mathbf{q}\times\mathbf{p}\cdot(\boldsymbol{\sigma}_1+\boldsymbol{\sigma}_2)(\tau_{10}+\tau_{20})\right.\\&\left.+6\left[\frac{k^2}{3}-\frac{q^2}{4}\right]i\mathbf{q}\times\mathbf{p}\cdot(\boldsymbol{\sigma}_1-\boldsymbol{\sigma}_2)(\tau_{10}-\tau_{20})+\frac{8}{9}k^2(i\mathbf{q}\times\mathbf{p})\cdot(\boldsymbol{\sigma}_1\times\boldsymbol{\sigma}_2)(\boldsymbol{\tau}_1\times\boldsymbol{\tau}_2)_0\right].\end{aligned}\tag{19}$$

In these equations only the numerators depicting the spin-isospin structure are expressed. The energy denominators

TABLE II. The space-spin structures of different diagrams for vertices H_2 and H_2'. The coefficients $A^{\pm}$, B, C, and D are as defined in Eq. (17).

5(a)	$-A^-$	$+2C\mathbf{q}\times\mathbf{p}\cdot\boldsymbol{\sigma}_1$	$-B\mathbf{q}\times\mathbf{p}\cdot\boldsymbol{\sigma}_2$	$-D(\mathbf{q}\times\boldsymbol{\sigma}_1)\cdot(\mathbf{p}\times\boldsymbol{\sigma}_2)$
6(a)	$-A^-$	$-2C\mathbf{q}\times\mathbf{p}\cdot\boldsymbol{\sigma}_1$	$-B\mathbf{q}\times\mathbf{p}\cdot\boldsymbol{\sigma}_2$	$+D(\mathbf{q}\times\boldsymbol{\sigma}_1)\cdot(\mathbf{p}\times\boldsymbol{\sigma}_2)$
5(b)	$-A^-$	$+2B\mathbf{q}\times\mathbf{p}\cdot\boldsymbol{\sigma}_1$	$-C\mathbf{q}\times\mathbf{p}\cdot\boldsymbol{\sigma}_2$	$-D(\mathbf{p}\times\boldsymbol{\sigma}_1)\cdot(\mathbf{q}\times\boldsymbol{\sigma}_2)$
6(b)	$-A^-$	$+2B\mathbf{q}\times\mathbf{p}\cdot\boldsymbol{\sigma}_1$	$+C\mathbf{q}\times\mathbf{p}\cdot\boldsymbol{\sigma}_2$	$+D(\mathbf{p}\times\boldsymbol{\sigma}_1)\cdot(\mathbf{q}\times\boldsymbol{\sigma}_2)$
5(c)	$-A^-$	$-B\mathbf{q}\times\mathbf{p}\cdot\boldsymbol{\sigma}_1$	$+2C\mathbf{q}\times\mathbf{p}\cdot\boldsymbol{\sigma}_2$	$-D(\mathbf{p}\times\boldsymbol{\sigma}_1)\cdot(\mathbf{q}\times\boldsymbol{\sigma}_2)$
6(c)	$-A^-$	$-B\mathbf{q}\times\mathbf{p}\cdot\boldsymbol{\sigma}_1$	$-2C\mathbf{q}\times\mathbf{p}\cdot\boldsymbol{\sigma}_2$	$+D(\mathbf{p}\times\boldsymbol{\sigma}_1)\cdot(\mathbf{q}\times\boldsymbol{\sigma}_2)$
5(d)	$-A^-$	$-C\mathbf{q}\times\mathbf{p}\cdot\boldsymbol{\sigma}_1$	$+2B\mathbf{q}\times\mathbf{p}\cdot\boldsymbol{\sigma}_2$	$-D(\mathbf{q}\times\boldsymbol{\sigma}_1)\cdot(\mathbf{p}\times\boldsymbol{\sigma}_2)$
6(d)	$-A^-$	$+C\mathbf{q}\times\mathbf{p}\cdot\boldsymbol{\sigma}_1$	$+2B\mathbf{q}\times\mathbf{p}\cdot\boldsymbol{\sigma}_2$	$+D(\mathbf{q}\times\boldsymbol{\sigma}_1)\cdot(\mathbf{p}\times\boldsymbol{\sigma}_2)$
5(e)	A^+	$-2C\mathbf{q}\times\mathbf{p}\cdot\boldsymbol{\sigma}_1$	$+B\mathbf{q}\times\mathbf{p}\cdot\boldsymbol{\sigma}_2$	$-D(\mathbf{q}\times\boldsymbol{\sigma}_1)\cdot(\mathbf{p}\times\boldsymbol{\sigma}_2)$
6(e)	A^+	$+2C\mathbf{q}\times\mathbf{p}\cdot\boldsymbol{\sigma}_1$	$+B\mathbf{q}\times\mathbf{p}\cdot\boldsymbol{\sigma}_2$	$+D(\mathbf{q}\times\boldsymbol{\sigma}_1)\cdot(\mathbf{p}\times\boldsymbol{\sigma}_2)$
5(f)	A^+	$-2B\mathbf{q}\times\mathbf{p}\cdot\boldsymbol{\sigma}_1$	$+C\mathbf{q}\times\mathbf{p}\cdot\boldsymbol{\sigma}_2$	$-D(\mathbf{p}\times\boldsymbol{\sigma}_1)\cdot(\mathbf{q}\times\boldsymbol{\sigma}_2)$
6(f)	A^+	$-2B\mathbf{q}\times\mathbf{p}\cdot\boldsymbol{\sigma}_1$	$-C\mathbf{q}\times\mathbf{p}\cdot\boldsymbol{\sigma}_2$	$+D(\mathbf{p}\times\boldsymbol{\sigma}_1)\cdot(\mathbf{q}\times\boldsymbol{\sigma}_2)$
5(g)	A^+	$+B\mathbf{q}\times\mathbf{p}\cdot\boldsymbol{\sigma}_1$	$-2C\mathbf{q}\times\mathbf{p}\cdot\boldsymbol{\sigma}_2$	$-D(\mathbf{p}\times\boldsymbol{\sigma}_1)\cdot(\mathbf{q}\times\boldsymbol{\sigma}_2)$
6(g)	A^+	$+B\mathbf{q}\times\mathbf{p}\cdot\boldsymbol{\sigma}_1$	$+2C\mathbf{q}\times\mathbf{p}\cdot\boldsymbol{\sigma}_2$	$+D(\mathbf{p}\times\boldsymbol{\sigma}_1)\cdot(\mathbf{q}\times\boldsymbol{\sigma}_2)$
5(h)	A^+	$+C\mathbf{q}\times\mathbf{p}\cdot\boldsymbol{\sigma}_1$	$-2B\mathbf{q}\times\mathbf{p}\cdot\boldsymbol{\sigma}_2$	$-D(\mathbf{q}\times\boldsymbol{\sigma}_1)\cdot(\mathbf{p}\times\boldsymbol{\sigma}_2)$
6(h)	A^+	$-C\mathbf{q}\times\mathbf{p}\cdot\boldsymbol{\sigma}_1$	$-2B\mathbf{q}\times\mathbf{p}\cdot\boldsymbol{\sigma}_2$	$+D(\mathbf{q}\times\boldsymbol{\sigma}_1)\cdot(\mathbf{p}\times\boldsymbol{\sigma}_2)$

(nonrelativistic propagators) will be discussed later in Sec. II D.

As shown previously in Eq. (14) the box contribution can be treated by coupled channels leaving as the residual interaction

$$V_{\rm res}=-(N_B-N_C)D_C$$
$$=\left[\frac{ff^*}{\mu^2}\right]^2\frac{\delta}{3}\left[-\frac{1}{3}(16k^4-q^4)(\tau_{10}+\tau_{20})-\frac{16}{3}\left[\frac{k^2}{3}-\frac{q^2}{4}\right]i\mathbf{q}\times\mathbf{p}\cdot(\boldsymbol{\sigma}_1+\boldsymbol{\sigma}_2)(\tau_{10}+\tau_{20})\right.$$
$$\left.+\frac{16}{3}\left[\frac{k^2}{3}-\frac{q^2}{4}\right]i\mathbf{q}\times\mathbf{p}\cdot(\boldsymbol{\sigma}_1-\boldsymbol{\sigma}_2)(\tau_{10}-\tau_{20})\right]D_C\ . \tag{20}$$

The first two terms are of class III and of no immediate interest in the present work, whereas the last term is of class IV contributing to ΔA in np scattering. It is interesting to note that the charge exchange CSB force can be completely treated by coupled channels leaving a vanishing residual.

For nucleonic intermediate states the CSB TPE is

$$\text{box}=\left[\frac{f}{\mu}\right]^4\delta\left[4\left[\frac{k^2}{3}-\frac{q^2}{4}\right]i\mathbf{q}\times\mathbf{p}\cdot(\boldsymbol{\sigma}_1-\boldsymbol{\sigma}_2)(\tau_{10}-\tau_{20})+\frac{4k^2}{3}(i\mathbf{q}\times\mathbf{p})\cdot(\boldsymbol{\sigma}_1\times\boldsymbol{\sigma}_2)(\boldsymbol{\tau}_1\times\boldsymbol{\tau}_2)_0\right]\ , \tag{21}$$

$$\text{crossed}=\left[\frac{f}{\mu}\right]^4\delta\left[-8\left[k^4-\frac{q^4}{16}\right](\tau_{10}+\tau_{20})+4\left[\frac{k^2}{3}-\frac{q^2}{4}\right]i\mathbf{q}\times\mathbf{p}\cdot(\boldsymbol{\sigma}_1+\boldsymbol{\sigma}_2)(\tau_{10}+\tau_{20})\right.$$
$$\left.+\frac{4k^2}{3}(i\mathbf{q}\times\mathbf{p})\cdot(\boldsymbol{\sigma}_1\times\boldsymbol{\sigma}_2)(\boldsymbol{\tau}_1\times\boldsymbol{\tau}_2)_0\right]\ . \tag{22}$$

Of course, the boxes are normally obtained automatically by solving the Schrödinger equation. However, the stretched box diagrams similar to 4(e) and 4(f) with two simultaneous pions are not included in this way and should be added separately. Since there are many more crossed diagrams than stretched boxes with the same numbers of simultaneous pions, the crossed contribution may be expected to be larger and class IVa to dominate over IVb. This conclusion agrees with Ref. [6], though numerically the present result will become larger.

2. *Vertex H_1*

Similarly, Table III gives the operators and the corresponding matrix elements for the CSB πNN vertex of the type H_1 in Eq. (4) as shown in Fig. 7. There are fewer diagrams, since this vertex can only appear in the nucleon end of pion exchange. Again the zeros for the matrix elements of the box diagrams are obvious. The zeros of the crossed diagrams are not so immediately obvious but still understandable. Since this CSB vertex does not change the baryon isospin state (no τ operator), from the point of view of the initial state the crossed graphs 7(a) and 7(b) effectively look like a CS transition potential into an $N\Delta$ or ΔN intermediate state, and this is nonzero only for a $T=1$ state because of isospin conservation. On the other hand, the space-spin part for the H_1 generated CSB potential is the same as for the isospin respecting interaction. The terms in Eq. (11) are totally symmetric in the exchange of the N and the Δ. Obviously then the sum of all the diagrams in Fig. 7 would give only an isospin conserving class III force and would not mix the isospin, once the isospin factors of Table III are taken into account.

However, also this type of vertex (due to either the np mass difference or $\eta\pi$ mixing) was found to contribute significantly to the effective class IV interaction and ΔA in the coupled channels calculations of Ref. [24]. Qualitatively one could understand this, because in individual partial waves the spin changing matrix elements do not vanish. Due to different distortions then their cancellation is not complete. On a more quantitative basis the explanation is that, in fact, there is an additional term in the spin-space numerator of the box diagrams, which is *not* symmetric in the exchange of the nucleon and the Δ:

TABLE III. The isospin factors $\boldsymbol{\tau}_1\cdot\boldsymbol{\phi}\phi_0\mathbf{T}_2^\dagger\cdot\boldsymbol{\phi}\mathbf{T}_2\cdot\boldsymbol{\phi}$ etc. for the CSB vertex of the type H_1 of Eq. (4).

Diagram	Box		Crossed	
	Operator	$\langle 10\|Op\|00\rangle$	Operator	$\langle 10\|Op\|00\rangle$
7(a)	$\frac{2}{3}\tau_{10}+\frac{i}{3}(\boldsymbol{\tau}_1\times\boldsymbol{\tau}_2)_0$	$\frac{4}{3}$	$\frac{2}{3}\tau_{10}-\frac{i}{3}(\boldsymbol{\tau}_1\times\boldsymbol{\tau}_2)_0$	0
7(b)	$\frac{2}{3}\tau_{20}-\frac{i}{3}(\boldsymbol{\tau}_1\times\boldsymbol{\tau}_2)_0$	$-\frac{4}{3}$	$\frac{2}{3}\tau_{20}+\frac{i}{3}(\boldsymbol{\tau}_1\times\boldsymbol{\tau}_2)_0$	0
7(c)	$\frac{2}{3}\tau_{10}-\frac{i}{3}(\boldsymbol{\tau}_1\times\boldsymbol{\tau}_2)_0$	0	$\frac{2}{3}\tau_{10}+\frac{i}{3}(\boldsymbol{\tau}_1\times\boldsymbol{\tau}_2)_0$	$\frac{4}{3}$
7(d)	$\frac{2}{3}\tau_{20}+\frac{i}{3}(\boldsymbol{\tau}_1\times\boldsymbol{\tau}_2)_0$	0	$\frac{2}{3}\tau_{20}-\frac{i}{3}(\boldsymbol{\tau}_1\times\boldsymbol{\tau}_2)_0$	$-\frac{4}{3}$

$$\Delta N_2(\text{odd}) = \left[\frac{ff^*}{\mu^2}\right]^2 \delta \left[\frac{i}{3}\left[k^2-\frac{q^2}{4}\right](2\mathbf{q}\times\mathbf{k}\cdot\boldsymbol{\sigma}_1-\mathbf{q}\times\mathbf{k}\cdot\boldsymbol{\sigma}_2)\right],$$
$$\Delta N_1(\text{odd}) = \left[\frac{ff^*}{\mu^2}\right]^2 \delta \left[\frac{i}{3}\left[k^2-\frac{q^2}{4}\right](-\mathbf{q}\times\mathbf{k}\cdot\boldsymbol{\sigma}_1+2\mathbf{q}\times\mathbf{k}\cdot\boldsymbol{\sigma}_2)\right], \tag{23}$$

where the subscripts refer to the particle that goes through the Δ intermediate state. [ΔN_2 corresponds to Figs. 7(a) and 7(c), ΔN_1 to 7(b) and 7(d).] This is odd in the integration variable $\mathbf{k}$ and has been omitted previously. It was already mentioned that for box diagrams there is also an odd contribution in the energy denominators due to the intermediate baryon energies. In principle, then these two odd terms can be combined to give a total nonzero effect, which does not actually vanish in the angular integration over the intermediate momentum but could be small in the above case of vertex H_2 in a comparison with the dominant isotropic background. Now, since the background gives a zero contribution, it is necessary to calculate this higher-order term from the angular dependence.

Simply combining the space-spin parts of Eqs. (11) and (23) with the isospin factors of Table III and performing the angular integration over $\mathbf{k}$, one gets the isospin nonsymmetric result for the sum of diagrams 7(a)–7(d) as

$$\text{box} = \left[\frac{ff^*}{\mu^2}\right]^2 \delta \left\{\frac{4}{9}\left[2\left[k^2-\frac{q^2}{4}\right]^2+\frac{k^2q^2}{9}\left[2\boldsymbol{\sigma}_1\cdot\boldsymbol{\sigma}_2-S_{12}\right]+\epsilon\frac{k^2}{6}\left[k^2-\frac{q^2}{4}\right]i\mathbf{q}\times\mathbf{p}\cdot(\boldsymbol{\sigma}_1+\boldsymbol{\sigma}_2)\right](\tau_1+\tau_2)_0\right.$$
$$\left.+\epsilon\frac{2k^2}{9}\left[k^2-\frac{q^2}{4}\right]i\mathbf{q}\times\mathbf{p}\cdot(\boldsymbol{\sigma}_1-\boldsymbol{\sigma}_2)(\tau_1-\tau_2)_0\right\}, \tag{24}$$

$$\text{crossed} = \left[\frac{ff^*}{\mu^2}\right]^2 \delta \left\{\frac{4}{9}\left[2\left[k^2-\frac{q^2}{4}\right]^2-\frac{k^2q^2}{9}(2\boldsymbol{\sigma}_1\cdot\boldsymbol{\sigma}_2-S_{12})\right](\tau_1+\tau_2)_0\right\}. \tag{25}$$

The parameter $\epsilon(k,p)$ is in fact connected rather to the propagator of the particular time ordering, but is symbolically included here with the numerator to remind which terms require this special treatment of the angular dependence. It will be presented explicitly later, when the propagators are discussed.

A class IV force due to H_1 arises only in the box diagrams. Since in the crossed diagrams all $\mathbf{k}$ dependence of the propagators combines to form an even function, no class IV interaction survives there in the integration over intermediate momenta. Since the angular dependence of the propagators of the box can cause a nonzero result in spite of the pure numerator of the form involving only a "class III" vertex (i.e., H_1, not "class IV" H_2 or H_2'), then the nonzero result for isospin mixing from the coupled channels can now be understood. The energy denominators correspond to the Hamiltonians of the $N\Delta$ channels in the coupled Schrödinger equation. Since different partial waves have different centrifugal barriers, on partial wave basis the contributions from different intermediate isobar states cannot exactly cancel as they would, if the propagators were the same for all. Also the correlations generated by the strong interactions would be somewhat different in different channels. It is essential to realize that in partial waves the spin-isospin factors of isospin breaking $NN\leftrightarrow N\Delta$ transitions do *not* vanish for individual channels. Finally, it should be noted that class IV forces do not arise from any kind of boxes involving the vertex H_1 and only nucleons. The direct box is merely an iteration of the isospin conserving class III interaction and the crossed diagrams do not contribute either.

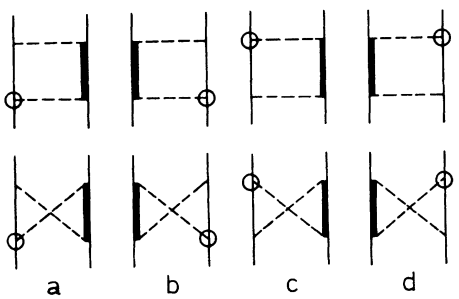

FIG. 7. Possible contributions of the CSB vertex H_1 [see Eq. (4)] to TPE involving the $N\Delta$ intermediate state. CSB can take place only in the nucleonic vertices.

In all the above results also the CSB interactions of class III are shown for later reference, although they will not be elaborated more in the present work which concentrates on *np* scattering. Since the vertex H_1 is similar to the isospin symmetric vertex H_0 in its spatial structure and since class III interactions are similar to isoscalar interactions, one can see that in second order of also normal charge-independent pion exchange one should get an induced effective spin-orbit force from box diagrams, although this is in no way apparent in the basic interactions. This has been demonstrated elsewhere, for example, in the spectacularly large polarization in $\bar{p}p$ scattering due to the very strong tensor force of the $T=0$ $\bar{N}N$ interaction [27].

D. Propagators

Now we turn to the nonrelativistic propagators. In the static limit for the baryons it is very straightforward to see that the sum of all propagators in Fig. 4 reduces to

the form $-(\omega_1\omega_2\Delta M)^{-1}$, where ΔM is the mass difference between the Δ and the electron. With the normalization factors of the pion fields this gives a result which is exactly as if a normal OPE (with range μ^{-1}) had been iterated with an intermediate state of the excitation energy $E_i - E = \Delta M$. In fact, even the static limit is unnecessarily restrictive and can be extended to an accuracy to which the approximation

$$E-\tilde{E}_{\mathbf{p}-\mathbf{k}}=(E-\tilde{E}_{\mathbf{p}+\mathbf{k}})+(E-E_{\mathbf{p}-\mathbf{k}}) \tag{26}$$

is valid, where $2E$ is the total incident c.m. energy, $E_{\mathbf{p}-\mathbf{k}}$ the intermediate nucleon energy, and $\tilde{E}$ the Δ energy. As if each nucleon is assumed to carry the energy E in the external states (i.e., the elastic situation). Here the nucleon and meson intermediate energies are

$$\begin{aligned} E_1&=\sqrt{M^2+(\mathbf{p}-\mathbf{k})^2}, \quad \omega_1=\sqrt{\mu^2+(\mathbf{k}-\mathbf{q}/2)^2}\,, \\ E_2&=\sqrt{M^2+(\mathbf{p}+\mathbf{k})^2}, \quad \omega_2=\sqrt{\mu^2+(\mathbf{k}+\mathbf{q}/2)^2}\,. \end{aligned} \tag{28}$$

The analogous Δ energy is denoted by $\tilde{E}_i$ $(i=1,2)$ and has the Δ mass instead of the nucleon mass. In spite of the nonrelativistic perturbation theory, the energies can be taken as relativistic. Except for the purpose of deriving the form of one part of the interaction in terms of $i\mathbf{q}\times\mathbf{p}$ in Sec. II C, the external kinetic energy E is omitted in the calculation of the propagators. (Note also that in this limit $\mathbf{p}\to\mathbf{q}/2$ and $i\mathbf{q}\times\mathbf{p}\to 0$, as it should, because it represents the orbital angular momentum.) The total potential in the momentum presentation is then obtained by calculating the integral

$$V(\mathbf{q})=\int \frac{d^3k}{(2\pi)^3}(N_B D_B + N_C D_C)\,. \tag{29}$$

Partial potentials are calculated similarly using the same conventions.

To calculate the angular dependence correction to the box diagrams, the intermediate energies E_i and $\tilde{E}_i$ are expanded in powers of $\mathbf{k}\cdot\mathbf{p}$ keeping only two lowest orders. compared with the mass difference of the nucleon and the Δ ($\approx$ the first term) the last term can often reasonably be ignored in an integration over $\mathbf{k}$. Due to this property of the propagators it is convenient to perform the division (14) into a term which can be calculated by iterating the transition potential plus a potential term. Of these, the first one can be expected to have a strong energy dependence around the Δ threshold and is treated exactly by coupled channels. The second one depends on the energy more smoothly and is developed as a two meson exchange potential at the NN threshold.

The propagators can be explicitly written as sums of the energy denominators of different time orderings

$$\begin{aligned} D_B=&\left[\frac{1}{(E-E_1-\omega_2)(2E-E_1-\tilde{E}_1)(E-E_1-\omega_1)}+\frac{1}{(E-E_1-\omega_2)(2E-E_1-\tilde{E}_1)(E-\tilde{E}_1-\omega_1)}\right.\\ &+\frac{1}{(E-\tilde{E}_1-\omega_2)(2E-E_1-\tilde{E}_1)(E-E_1-\omega_1)}+\frac{1}{(E-\tilde{E}_1-\omega_2)(2E-E_1-\tilde{E}_1)(E-\tilde{E}_1-\omega_1)}\\ &\left.+\frac{1}{(E-E_1-\omega_2)(-\omega_1-\omega_2)(E-\tilde{E}_1-\omega_1)}+\frac{1}{(E-\tilde{E}_1-\omega_2)(-\omega_1-\omega_2)(E-E_1-\omega_1)}\right]\frac{1}{4\omega_1\omega_2}\,,\\ D_C=&\left[\frac{1}{(E-E_1-\omega_2)(2E-E_1-\tilde{E}_2-\omega_1-\omega_2)(E-E_1-\omega_1)}+\frac{1}{(E-E_1-\omega_2)(2E-E_1-\tilde{E}_2-\omega_1-\omega_2)(E-\tilde{E}_2-\omega_2)}\right.\\ &+\frac{1}{(E-\tilde{E}_2-\omega_1)(2E-E_1-\tilde{E}_2-\omega_1-\omega_2)(E-E_1-\omega_1)}+\frac{1}{(E-\tilde{E}_2-\omega_1)(2E-E_1-\tilde{E}_2-\omega_1-\omega_2)(E-\tilde{E}_2-\omega_2)}\\ &\left.+\frac{1}{(E-E_1-\omega_2)(-\omega_1-\omega_2)(E-\tilde{E}_2-\omega_2)}+\frac{1}{(E-\tilde{E}_2-\omega_1)(-\omega_1-\omega_2)(E-E_1-\omega_1)}\right]\frac{1}{4\omega_1\omega_2}\,, \end{aligned} \tag{27}$$

The correction to each factor of a given time ordering term is $-\mathbf{k}\cdot\mathbf{p}$ times this factor multiplied with the sum of the inverses of the appropriate energies included in this factor. So, for example, the first term in the box propagator becomes in this way

$$\begin{aligned} D_{B1}\to D_{B1}\left\{1-\mathbf{k}\cdot\mathbf{p}\left[\frac{1}{E_1}\frac{1}{E-E_1-\omega}\right.\right.&+\left[\frac{1}{E_1}+\frac{1}{\tilde{E}_1}\right]\frac{1}{E-E_1-\tilde{E}_1}\\ &\left.\left.+\frac{1}{E_1}\frac{1}{E-E_1-\omega_1}\right]\right\}. \end{aligned} \tag{30}$$

Angular integration with the numerator (23) gives then the result (24) and (25) for the effective CSB potential. The above additional correction term in the square brackets is what was symbolically denoted by ϵ and is actually part of the propagator resulting also in different radial dependence.

When the energy dependence is essential, especially near the $N\Delta$ threshold, the coupled channels approach can be used. This amounts to coupled Schrödinger equations of the type

$$(-\nabla^2/M+V_{NN}-E)\Psi_{NN}=-V_{\rm tr}\Psi_{N\Delta}\ ,$$
$$(-\nabla^2/2M_{\rm red}+V_{N\Delta}+\Delta-M-E)\Psi_{N\Delta}=-V_{\rm tr}\Psi_{NN}\ , \tag{31}$$

where $M_{\rm red}=M\Delta/(M+\Delta)$ is the $N\Delta$ reduced mass. The transition potential $V_{\rm tr}$ contains in addition to pion exchange also ρ meson exchange. Apparently the energy dependence of the $N\Delta$ propagator is closely related to the energy vs the mass difference $\Delta-M$ in the second equation. Pionic inelasticities can be handily incorporated by inclusion of the Δ width making its mass complex [28]. In partial waves the centrifugal barrier can be different for different $N\Delta$ states coupled to the same NN initial state, causing, e.g., isospin breaking also for the type H_1 CSB vertex as was found earlier in Ref. [24]. As noted above, the total sum of all the propagators would correspond to a second-order iteration of the OPE transition potential $V_{\rm tr}$ at least in the static baryon limit. However, since the numerators are not the same for the crossed and box diagrams, a modification is necessary as shown in Eq. (14). In principle, the effective potential could be computed for finite energies. However, the use of such an energy-dependent potential would be cumbersome, since it should be computed for each energy as a three-dimensional integral. Clearly the coupled channels method is preferable as a way of introducing energy dependence. In the low-energy limit the two methods were shown to give numerically similar results. As a bonus the coupled channels give the explicit $N\Delta$ wave function for use in reactions etc., when there is an external probe on the details of the baryon wave functions.

Finally, it may be noted that since the charge is conserved, in the quark model the overall mass of the intermediate state M_N+M_Δ remains independent of the individual charges of the Δ or the nucleon (i.e., the number of u and d quarks is constant). This means that the total mass difference between the NN and $N\Delta$ states is charge independent and does not cause isospin breaking. It is the charge dependence of the *individual* baryon mass at the meson-baryon vertex considered above that breaks the isospin symmetry. Further, in the case of neutron-proton scattering one of the baryons is always neutral, so there is no long-range Coulomb interaction adding to the propagators. Therefore, the propagators themselves do not break charge symmetry. Also any isospin breaking interaction in the $N\Delta$ intermediate state can be neglected, because the only isospin change could be from $T=1$ to $T=2$ states, which would require another isospin violating interaction to connect to a two nucleon state. So it can be concluded that it is sufficient to consider only the CSB mechanisms introduced to the numerator in the previous subsections.

III. RESULTS

The two-pion exchange potentials described in Sec. II are calculated in the momentum space in the static approximation, where all baryon energies are neglected. Also some results are given to show the possible influence of nonstatic effects, by calculating the TPE potential including the intermediate state baryon energies but still neglecting all external energies. Figure 8 shows the isobar contributions to the class IV CSB interactions in the static model. Both the part treatable by coupled channels and $V_{\rm res}$ are calculated at the initial zero energy. The solid curves are the result of numerical integration and the overlapping dotted lines are fits with functions of the type

$$V(q)=A\frac{B^2}{B^2+q^2}\left[\frac{C^2}{C^2+q^2}\right]^n\quad(n=0,1,2)\ . \tag{32}$$

Since the fit is so good that it cannot be distinguished from the exact results, apparently the two-pion exchange potential (TPEP) can be well approximated in the coordinate space by a single Yukawa function modified by a monopole or dipole form factor. This is a significant simplification in numerical calculations, when TPEP is used. The irreducible TPE with nucleonic intermediate states can be parametrized similarly.

Table IV gives the results of this fitting for different potential components with the notation $V_i(j)=\int[d^3k/(2\pi)^3]k^iD_j$. (The coupling constants and other coefficients are not included in these fitting parameters.) The potentials $V_0(j)$ (and V_2 for the angular correction), which in the present context appear with an additional factor q^2, were fitted with this as a weight function. The values of the masses B from unweighted fits are generally 5% lower and the form-factor masses C 5–7 % higher, so the results are not excessively dependent on the fitting procedure. Also V_4 is given for completeness, since these ingredients can be used to build a class III or isospin symmetric TPEP. Furthermore, it should be added that in this calculation also a monopole form factor

$$F(q)=\frac{\Lambda^2-\mu^2}{\Lambda^2+q^2} \tag{33}$$

is included in each pion-baryon vertex. [However, to avoid superficial normalization factors in the results of Table IV the normalization with Λ^2 in the numerator, i.e., $F(0)=1$, is used.] The value of the cutoff mass Λ is taken to be 1000 MeV. This is a reasonable compromise

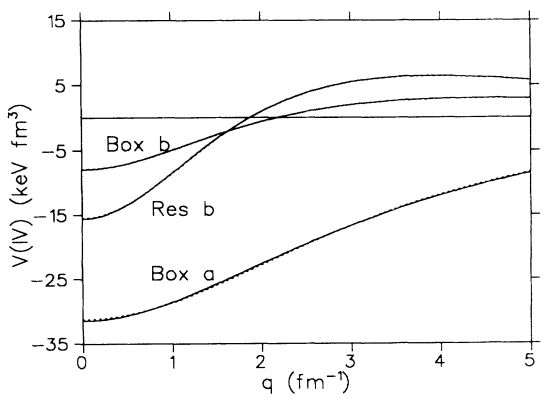

FIG. 8. Contributions from different isobar effect parts to the class IVa and IVb CSB potentials in the momentum space. Here "box" means the first term of Eq. (14), which can be obtained by iterating normal pionic transition potential.

TABLE IV. Parametrizations for potentials $V_i(j)$ as described in the text. Here in the form factor $n=2$ for V_0 and $n=1$ for V_2, whereas V_4 has no form factor. All A's are given in the units of MeV fm^{3-i} and B's and C's in fm^{-1}. These need the appropriate coupling constants and other numerical factors shown in Eqs. (18)–(26) to make the actual physical potentials.

	A_0	B_0	C_0	A_2	B_2	C_2	A_4	B_4
$\Lambda=1000$ MeV								
$N\Delta$ cross	−1.426	1.973	6.411	−2.368	3.200	8.635	−14.60	4.786
$N\Delta$ box	−3.021	2.267	7.577	−7.200	3.745	9.468	−66.80	5.384
NN cross	−3.905	1.689	6.005	−4.861	2.830	9.228	−23.51	4.720
NN "long"	−1.310	1.604	5.313	−1.624	2.603	6.707	−8.007	3.715
Angle				−2.715	3.788	8.184	−22.56	5.257
$\Lambda=790$ MeV								
$N\Delta$ cross	−1.280	1.909	4.997	−1.722	2.837	6.079	−7.682	3.774
$N\Delta$ box	−2.635	2.113	5.828	−4.773	3.222	6.831	−30.28	4.260
NN cross	−3.579	1.660	4.680	−3.729	2.515	6.250	−13.25	3.664
NN "long"	−1.195	1.605	4.201	−1.244	2.399	4.721	−4.506	2.969
Angle				−1.884	3.276	5.905	−10.65	4.131
Nonstatic $\Lambda=790$ MeV								
$N\Delta$cross	−1.113	1.866	4.039	−1.290	2.842	3.870	−4.852	2.909
$N\Delta$ box	−2.052	1.901	4.479	−2.620	2.642	5.210	−10.13	3.283
NN cross	−2.970	1.594	3.493	−2.549	2.372	3.533	−7.261	2.550
NN "long"	−1.056	1.525	3.726	−0.961	2.213	4.056	−2.949	2.610
Angle				−0.832	2.230	5.034	−2.112	3.085

between soft [29] and hard [30] form factors of 700–800 and 1200–1300 MeV, respectively, and will be given further justification as giving the correct $NN\to N\Delta$ transition potential strength in pion production. From the table it is immediately seen that the range of the TPEP is somewhat longer than that of vector mesons, making it potentially important if the effective couplings are strong enough.

The solid curves in Fig. 9 show the contributions of the $N\Delta$ mechanism to the CSB TPE interaction in the coordinate presentation. Since class IVa and IVb potentials become comparable outside 1 fm, at low energy γ_1 should become negligible because of cancellation, whereas γ_2 remains large. In addition to the isobar effects, Fig. 9 presents also the irreducible CSB TPE potential arising from the nucleonic time orderings which are not obtained simply by iterating the OPE (dashed curves). The effective charged exchange is nearly as important as with Δ's. A specific note may be in place about the sign change of the two IVb potentials. Formally one would expect the terms proportional to k^2 and q^2 in Eqs. (18)–(22) to add constructively, because operating on a Yukawa function q^2 should give just a factor $-B_0^2$. However, the dipole form factor in the potential V_0 is so strong that it dominates this term inside the OPE range, causing strong cancellation of the two terms and changing the sign of the class IVb potentials at 0.8 fm. The strong effect of the form factor may be the reason why the nucleonic contribution here is significantly larger than that obtained in Ref. [6], where the two class IV interactions nearly cancelled each other at the crossover angle. The corresponding term in the potential derived from the angular correction [Eq. (24)] has only a monopole form factor of shorter range and is also proportionally smaller, so that this class IVb potential remains significant at intermediate ranges. For comparison also the OPE contribution is shown (dotted curve). Inside about 1 fm radius the TPE potentials become significant and should be given serious consideration at medium and high energies.

Table IV shows also the potentials using the nonstatic model results and for a softer form factor with $\Lambda=790$ MeV. It can be seen that, although the general features are the same, the intermediate baryon energies may play

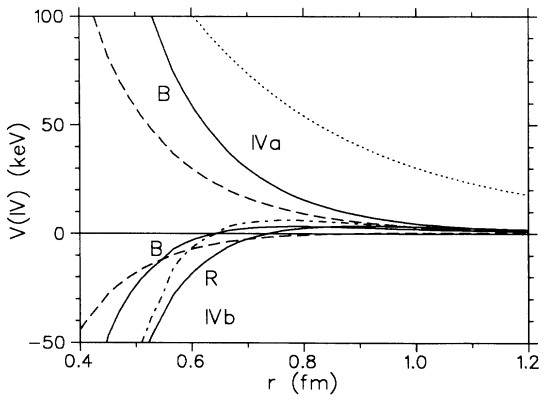

FIG. 9. The TPE contributions to the class IVa and IVb CSB potentials in the coordinate representation. Solid lines: the isobar contributions as in Fig. 8. B refers to "box" and R to "residual." Dashed lines: the nucleon intermediate states not obtained by iterating OPE. Chain line: the contribution from the isobar box angular correction as discussed in Sec. II C 2. Also shown is the class IV OPE CSB potential of Eq. (7) (dotted line). All class IVa potentials remain positive, while those of class IVb become negative at short distances.

a significant role. Especially in the cases where a power of k is involved in the phase space integral, the nonstatic result differs from the static one, since high momenta are weighted and baryon energies cannot be neglected. One feature of these results is that the range in the present nonstatic model is longer than in the static model (the mass parameters B are smaller). This is somewhat unexpected since with the intermediate baryon energies the intermediate states should be further off mass shell. However, the longer range arises from the faster decrease of the propagators in this case, while the larger energy denominator is reflected in the smaller overall strength. Since the inclusion of baryon energies opens many new questions (e.g., nonstatic effects in exchanges of one meson) and different possible approximation schemes (this model of omitting all external energies in both the initial *and* the final state being just one), in the present calculations the static model is conservatively used, with this nonstatic result given only as a precaution and for completeness.

The isobar TPE contributions of the "box" type to the mixing parameters γ_1 and γ_2 are shown in Fig. 10. The solid curve is the part of the static model potential due to the isobar intermediate states that can be calculated by iterating the $NN \rightarrow N\Delta$ OPE transition potential of normal range [the first term in Eq. (14)]. Its behavior for partial waves with its sign alternating with J is similar to one-pion exchange, but an order of magnitude smaller. In all these TPE potential calculations the Reid soft core potential [19] is used to generate the two nucleon correlations.

In the following calculations the energy dependence will arise naturally in the coupled channels treatment of the dominant part of the TPE interaction, but would be clumsy to introduce into a potential. Since only crossed propagators appear in the residual interaction, its energy dependence is presumably much weaker than that of the box diagrams and is neglected. As a numerical test of the possible equivalence of the iterative boxlike potential of Eq. (14) and coupled channels, Fig. 10 shows a comparison of this contribution to the mixing parameters γ_1 and γ_2 calculated also by way of coupled channels in addition to the approximation by a TPE potential $N_B(D_B+D_C)$ computed at the zero energy. The agreement between the two methods at low energies (dotted vs solid curves) suggests that the potential approach is reasonable and should be even more reliable in the less energy-dependent residual interaction. At high energies the coupled channels results are significantly larger than the corresponding energy-independent TPE potential would give. The reason for this deviation is mostly due to the influence of the $N\Delta$ threshold. Also the interaction (Reid soft core potential modified to counteract the channel coupling effect on the phase shifts) was made phase equivalent with the original Reid potential only at 100 MeV, and the width of the $N\Delta$ state is included above pionic inelasticity threshold. The dotted curve presents the real part of the mixing parameter, which becomes complex in the presence of inelasticities [24]. In the present case (H_2') the imaginary part is small, since the operator $\mathbf{S}_1 \times \sigma_2 \cdot \mathbf{L}$ cannot connect $N\Delta$ states with lower L than in the initial state. The actively participating intermediate states are not favored in the transitions.

The situation is very different with the tensor transition potential part of $V_{\rm tr}$ of Eq. (10), which can arise from the use of both the charge-independent couplings and the CSB vertex H_1. With this a high orbital angular momentum initial state can get to a low L $N\Delta$ state. At the distance of 1 fm, most relevant for strong interactions, the gain in the centrifugal barrier energy can be comparable to the mass difference, resulting in an enhanced $N\Delta$ amplitude around this distance. Examples of transitions particularly important in the NN interaction are ${}^1D_2 \rightarrow {}^5S_2$, ${}^3F_3 \rightarrow {}^5P_3$, and ${}^1G_4 \rightarrow {}^5D_4$ "dibaryons." Section II C 2 indicated that this could be accounted for by a correction in the angular dependence of the propagator. Figure 11 shows now a comparison of mixing parameters for P waves (dashed curves) and D waves (solid curves) using the class IVb part of the potential (25) derived in Sec. II C 2 vs the coupled channels results. Again at low energies the two methods give qualitatively similar mixing parameters, while at and above the Δ threshold the coupled channels result is qualitative-

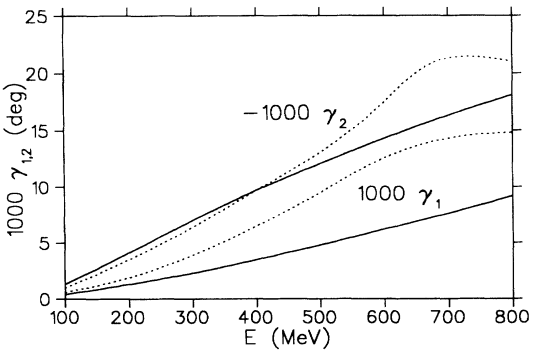

FIG. 10. The real parts of the mixing parameters γ_1 and γ_2 arising from H_2 and H_2' with $N\Delta$ excitations calculated by coupled channels (dotted) and by the corresponding zero energy box potential (solid).

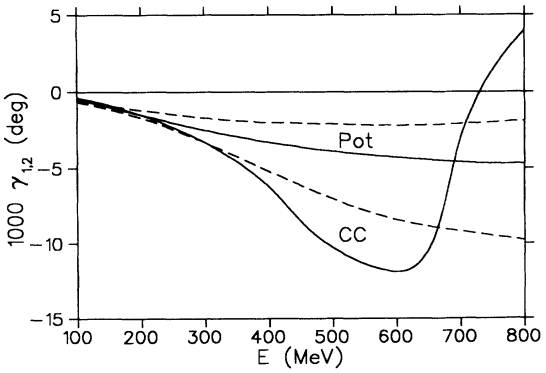

FIG. 11. Contributions to the mixing parameters γ_1 (dashed) and γ_2 (solid) arising from the H_1 vertex in the box diagrams of Fig. 7. The smaller ones are results from using the class IVb part of the potential (24), whereas the larger ones are obtained from a coupled channels calculation (the real parts of γ_J are shown).

ly larger. However, now it is important to remember that the figure shows only the real parts of coupled channels results. The $^5S_2$ and $^5P_3$ $N\Delta$ amplitudes go through a rapid resonancelike variation around their respective effective thresholds [31], and the imaginary parts are comparable to the real parts [24]. Quite apparently also this effect must be included in the consistent evaluation of TPE effects in charge symmetry breaking.

In the following calculations the coupled channels method will now always be used to treat the iterative part of the isobar contribution, and the effects of $V_{\rm res}$ and noniterative nucleon states will be added to the coupled channels results. Furthermore, also ρ exchange will be included in the isospin symmetric transition potential, so that equivalence of the pion box potential and coupled channels can no more be expected.

In the above consistency checks the diagonal NN interaction of the coupled system was the usual Reid soft core potential simply adjusted at intermediate range to produce the same phases at 100 MeV as the original. In the final calculations a better overall fit is used with also some short-range modifications added in both isospin states. To be precise, using the $N\Delta$ transition potential defined below the corrections to the Reid potential in the most important partial waves are (in MeV)

$$\begin{aligned}
\Delta V(^3P_1) &= -150\frac{e^{-3\mu r}}{\mu r} + 18\,000\frac{e^{-7\mu r}}{\mu r}\,, \\
\Delta V(^1P_1) &= 20\frac{e^{-2\mu r}}{\mu r} - 3100\frac{e^{-6\mu r}}{\mu r}\,, \\
\Delta V(^1D_2) &= 230\frac{e^{-3\mu r}}{\mu r} + 8000\frac{e^{-7\mu r}}{\mu r}\,, \\
\Delta V(^3D_2) &= 20\frac{e^{-3\mu r}}{\mu r} + 1500\frac{e^{-7\mu r}}{\mu r}\,.
\end{aligned} \tag{34}$$

In this way the $J=L$ phase shifts of the energy-dependent analysis of Ref. [32] can be reproduced to within three degrees over a wide energy range—only $^1D_2$ gets too attractive above about 700 MeV. However, these potentials are only used to give the distortions of the wave functions to calculate the mixing parameters γ_J. The strong interaction amplitudes of Ref. [32] are otherwise used to avoid introducing unessential theoretical error sources. As described in Ref. [8], the long-ranged OPE is subtracted in partial wave amplitudes and added back into the overall angle-dependent spin amplitudes to avoid truncation effects on the partial wave expansion. Also all the calculated mixing parameters have the relativistic correction factor [6] $(M/E_T)^2$, where E_T is the total energy of a nucleon in the center-of-mass system.

The form factors are important in the overall strength of the transition potential. This can be fixed most conveniently and reliably by the height of the pion production maximum at about 580 MeV in the reaction $pp \to d\pi^+$. Using for this the model of Ref. [33] with the ρNN coupling constants $g_\rho^2/4\pi = 0.55$ MeV and $K_\rho = 6.1$ (Ref. [34]) it was possible to reproduce this cross section with the above $\Lambda = 1000$ MeV for the pion and $\Lambda_\rho = 1050$ MeV for the ρ, not very far from the pion value but significantly smaller than the Bonn potential fit [30]. However, this is quite gratifying in that the ρ does not see a different nucleon than the pion, and is also consistent with the proton electromagnetic form factor. No potential is inserted for the diagonal $N\Delta$ interaction $V_{N\Delta}$.

Figures 12 and 13 show the final TPE mixing parameters γ_1 and γ_2 and their composition of different contributions as a function of energy. The dotted curves are the results of the coupled channels $N\Delta$ calculation only, analogous to (but not the same as) the dotted curves in Fig. 10. The residual interaction turns out to be about as important at low energies due to its long range and the large factor in Eq. (20) vs the factors in Eq. (18). At short distances $V_{\rm res}$ changes sign, and this diminishes its effect at high energies. It decreases γ_1, but enhances the value of the negative γ_2, i.e., is a negative contribution in both. Structurally this is similar to $\rho\omega$ mixing, but again an order of magnitude smaller and of opposite sign. The total isobar effect arising from H_2 and H_2' is shown by the dash-dotted curve. As expected previously, at low energies γ_1 is quite small. The noniterative TPE with nucleonic states is in turn similar to pion exchange, as anticipated in the end of Sec. II C 1, and significantly increases both γ_1 and γ_2 (in the former largely cancelling the effect of $V_{\rm res}$ and bringing the total essentially to the same result as the iterative isobar contribution; dashed curves). The total sum of the TPE potential mixings, also including the contribution from the H_1 vertex, is given by the solid curve. This part shows the important $^5S_2(N\Delta)$ threshold effect in the energy dependence of γ_2.

In Figs. 12 and 13 also the onset of the imaginary part is presented, since it is so closely related to the box diagrams with Δ's. It is clearly seen that the imaginary part gets contributions mainly from the direct coupling to the $N\Delta$ states. For the inelasticity, the isospin breaking tensor interaction due to H_1 is crucial. As a curiosity, to check the cancellation of the $N\Delta$ effect under this interaction, if the correlations had been the same in different channels, the L_Δ was set to $L=J$ in all $N\Delta$

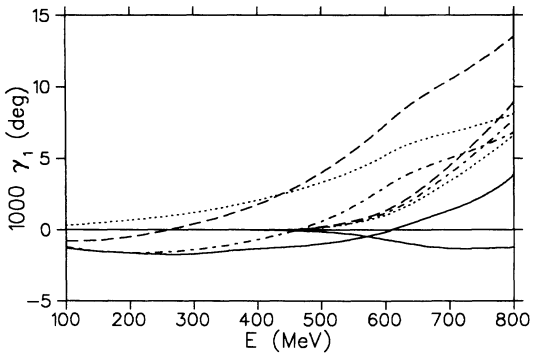

FIG. 12. The TPE contributions to the final mixing parameter γ_1: Dotted: Coupled channels result including Δ's with the vertex H_2'; dash-dotted: including also the residual interaction (20); dashed: including also the nucleonic intermediate states; solid: the total result, where also the transition potential arising from H_1 is used in the coupled channels calculation. The curves starting above 400 MeV are the imaginary parts, others the real parts.

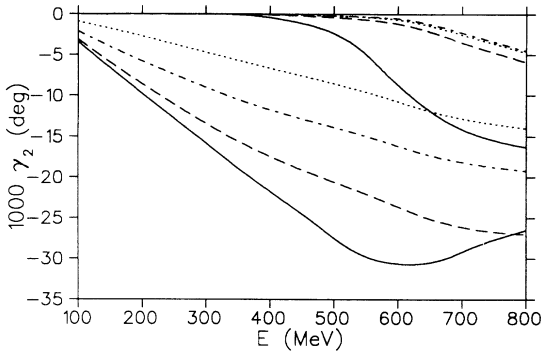

FIG. 13. As Fig. 12 but for γ_2.

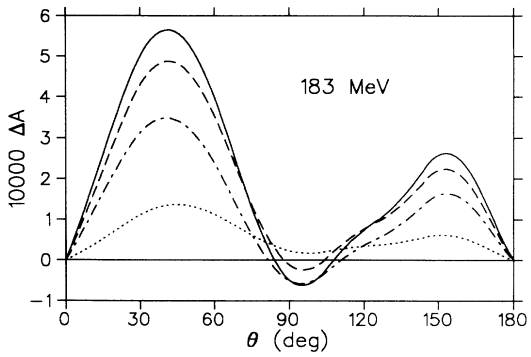

FIG. 15. As Fig. 14 but at 183 MeV.

channels. The result with more similar channel wave functions was indeed suppressed by an order of magnitude as compared with the above results, which confirms the conjecture presented in Sec. II C 2. Also inclusion or omission of any one channel in this exercise caused order of magnitude effects in the cancellation, even if a high angular momentum state was omitted.

In Figs. 14–17 the TPE effects to the observable $\Delta A(\theta)$ itself are given. Figures 14–16 have these split into various contributions as in Figs. 13 and 14. The corresponding energies are chosen to be the ones where there are data available [2,3] or an experiment is underway [4]. The division into single contributions is made to facilitate comparisons and combinations with other possible calculations of similar nature. Figure 17 shows the full TPE effect at four additional energies. These results show conclusively that at low energies TPE CSB can be neglected. It does not affect significantly the IUCF point at 183 MeV. However, it is an about 15% contribution at the TRIUMF energy 477 MeV and about 10% at 350 MeV. At higher energies also TPE is significant, though smaller than the dominant mechanisms. The reason for the relative smallness of TPE is that out of the four different contributions, roughly equal in magnitude, in γ_1 two pairs come with opposite signs. At the zero crossover angle of $A(\theta)$ this parameter is most decisive. Without this destructive interference the effect could have been twice as large. Outside the zero crossing angle (especially in the forward direction) the TPE contribution to ΔA is rather large.

Because the effect of TPE could, in principle, be larger than the result obtained above at the zero crossing angle (also indicated by the fact that *outside* this angle the contribution to ΔA is significant) a check of the dependence on the form factor is worthwhile. For this purpose the potentials with $\Lambda = 790$ MeV of Table IV were used in a coupled channels calculation. The isospin breaking transition potential had also the same form factors, but the stronger isospin symmetric one was kept as it was before. In spite of an apparent inconsistency at this point, physically there is little point to change the latter much, since its strength is dictated externally by the reaction $pp \to d\pi^+$. At intermediate energies the effect was to lower the TPE contribution to ΔA by 20–30 %, while at low energy (183 MeV) this came down by a factor of 3. The angular structure remained the same. Therefore, no qualitative change to the previous conclusions became necessary. Making the form factor harder would apparently effect the opposite way, except that the low-energy result would not change as drastically. Since the latter is so small at the crossover angle, the TPE effect remains still negligible at low energies. As observed also in Ref. [8], varying the form factors cannot qualitatively change the angular distribution and the forward maximum does not move towards the angle where experiments are possible.

Finally, in Fig. 18 is a study of the angular distribution of ΔA. Due to measurement uncertainty in the ratio of neutron to proton polarizations, $\Delta A(\theta)$ can be extracted from an experiment only to within a constant times

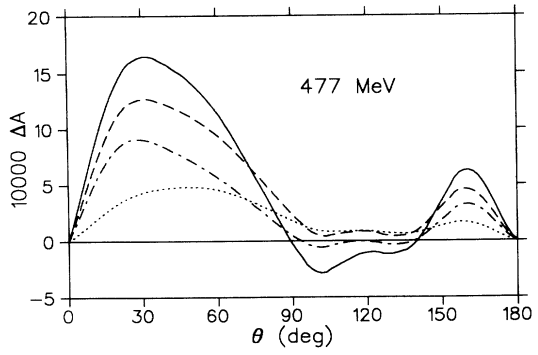

FIG. 14. TPE contributions to the observable $\Delta A(\theta)$ at 477 MeV. Notation as in Fig. 12.

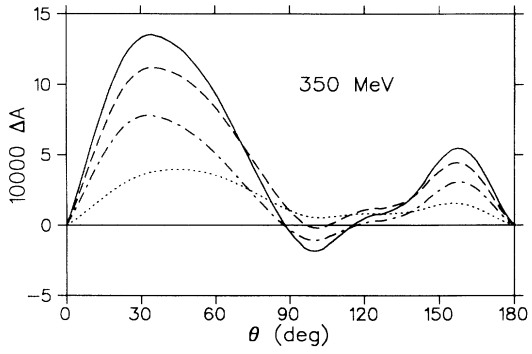

FIG. 16. As Fig. 14 but at 350 MeV.

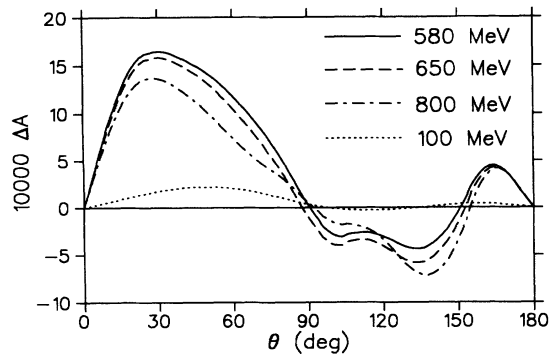

FIG. 17. The total TPE effect on $\Delta A(\theta)$ at four more energies.

$A(\theta)$, as indicated in Eq. (1) [3]. In the face of this ambiguity, a meaningful comparison between theory and experiment can still be made by considering the coefficient of $A(\theta)$ in Eq. (1) as a free parameter, adjusted to minimize the variance of $\Delta A(\theta)$ [3]. Effectively, this procedure determines a distribution $\Delta A(\theta)$ optimally orthogonal to $A(\theta)$ subject to the constraint (1). The same method has been applied in Fig. 18 for the present theoretical results at 183 MeV (Ref. [35]), using the same angle range (68°–121°) for the variance minimization as was used to obtain the experimental results [3]. Here are shown the results including OPE+γ+ρ (model 1, dash-dotted and dotted curves) and OPE+ρ+γ+$\rho\omega$+TPE (model 3, solid and dashed curves), the interest being in the effect of the $\rho\omega$ contribution. The curves without TPE at this energy are slightly lower in the forward direction but qualitatively indistinguishable. The full result changes little in going from the true $\Delta A(\theta)$ to the minimum variance modified distribution, but in the OPE result the change is more significant. The resulting full distribution agrees well with the similarly treated data, and is essentially indistinguishable from the one obtained from the Bonn results [7] in Ref. [3]. In calculating the CSB ρ and $\rho\omega$ contributions, the full Bonn potential couplings and form factors [30] are used, while the distorting potential is the full coupled channels calculation as described above.

Figure 19 shows a similar comparison of CSB effects for the true $\Delta A(\theta)$ and the modification due to the minimal variance at 350 MeV. (Here, an angle range 48°–96°, centered about the zero crossing angle at 350 MeV, has been used for the minimization.) Now the change of $\Delta A(\theta)$ from the minimal variance in the case of the total result is much larger than in Fig. 18 bringing the distribution close to OPE (which in turn remains practically unchanged). The reason for this large effect is the nearly complete correlation of the $\rho\omega$ effect with the analyzing power $A(\theta)$ itself at this energy, as was discussed in the Introduction. This shows that above, say, 300 MeV the only significant contributions to the minimal variance modified angular distribution must arise from class IVa forces, i.e., from charged exchanges. The minimal variance result without TPE at this energy would be about uniformly 0.0007 lower than the dashed curve shown here. At this point it could be added that

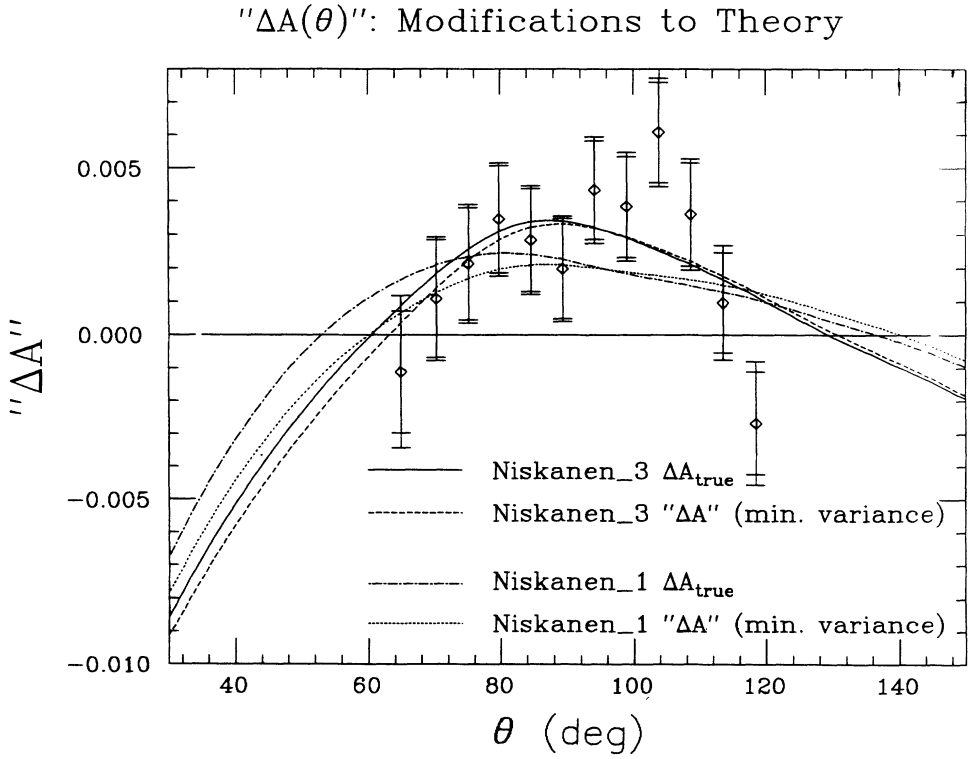

FIG. 18. The true and minimal variance modified angular distributions of $\Delta A(\theta)$ at 183 MeV. 1 refers to OPE+γ+ρ contributions, 3 to the total of all (OPE+ρ+γ+$\rho\omega$+TPE). The data are from Ref. [3].

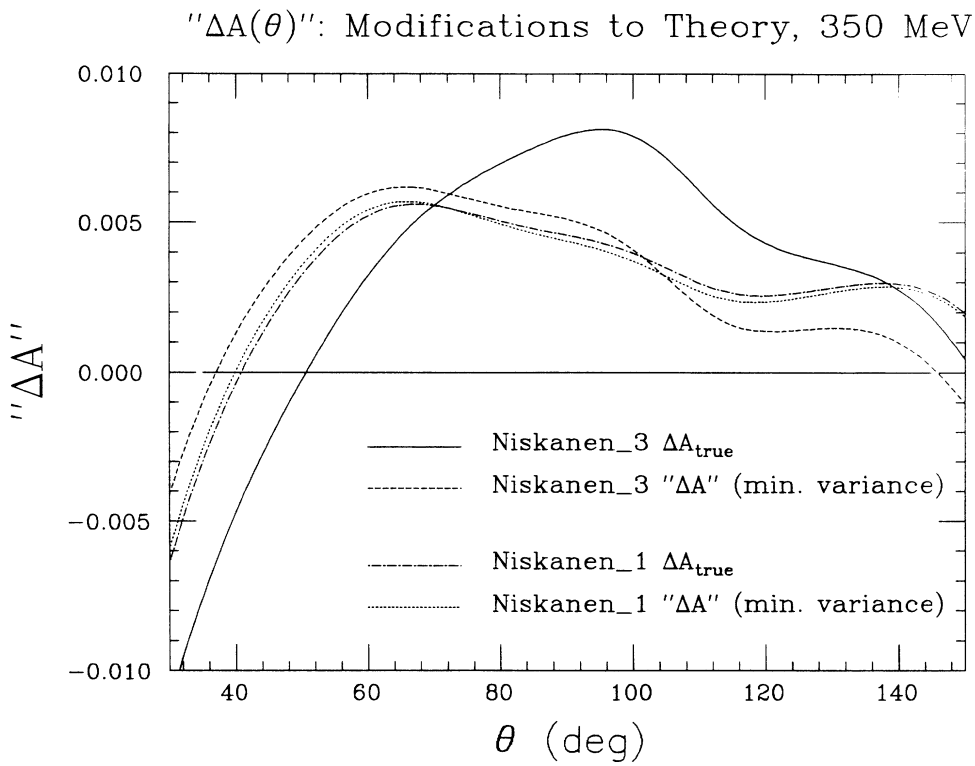

FIG. 19. As Fig. 18 but at 350 MeV.

the program SCORE [36], used in these calculations for Figs. 18 and 19, does not allow for inelasticity even in charge symmetric NN amplitudes (which is included in all other results of this paper). Since this program has been widely used in recent theoretical work on CSB [6,9] and also some other work [7] is elastic by construction, the neglect of inelasticity above the pion production threshold deserves an explicit study [37].

IV. CONCLUSION

In summary, a systematic study of class IV CSB in TPE has been made including both the NN and $N\Delta$ intermediate states. It can be seen that the energy dependence in the box diagrams is rather crucial and apparently a coupled channels treatment of the effect is preferable. However, far below the $N\Delta$ threshold an energy-independent TPE potential is found to be a reasonable approximation to the more exact approach. A division into two parts, in one of which the coupled channels method is applicable and the other a residual interaction with its propagator as in crossed diagrams, was introduced and employed in the calculations. In the particular case of class IV interactions the residual part was not small. This approach can be applied also more generally in charge-independent interactions and in the case of class III CSB [38]. A practical parametrization of TPE potentials is given in Table IV.

TPE does not change earlier interpretations of the available two data points at 183 MeV and at 477 MeV. The latter is dominated by OPE and the error limits are wide enough to allow the present 10–15 % TPE contribution to be added. At the lower energy TPE is negligible as compared with OPE, $\rho\omega$ meson mixing, and γ exchange. The proposed TRIUMF experiment at 350 MeV would be about intermediate also in the importance of TPE. The smallness of the effect is partly due to cancellations between individual contributions of roughly the same size. From the formalism of Sec. II C one may expect the $N\Delta$ effect to be of equal importance as TPE with nucleonic intermediate states (calculated in Ref. [16]) in the case of class III, but still an explicit calculation should and could easily be done for the difference of the singlet scattering lengths $\Delta a = a_{pp} - a_{nn}$ [38]. The formulas in Sec. II C and the parametrization of TPE potentials in Table IV can also be used as a starting point for calculating CSB in nuclei.

This work has evaluated one group of contributions of potential importance to CSB as a precaution in interpreting the data. There are other effects which also have a long range and should be incorporated for consistency. The mixing of the pion and the η meson gives rise to similar transition potentials as the vertex H_1 does [20,24]. This can be considered as long ranged since basically the η acts as if it were a soft form factor in OPE. The tensor coupling will be important in the mixing of the D states around the Δ threshold energy. Reference [24] treated only box diagrams which appears justified, since the effect is formally similar to that arising from H_1 discussed in Sec. II C 2, and so the crossed box contribution should be expected to be zero. However, the ηNN coupling constant remains a great source of uncertainty in this effect. Another long-ranged effect is the combined pion and γ exchange. It has been shown to be significant in the cases

of the isotensor interaction [16], giving 20% of the scattering length difference $\Delta a = (a_{pp} + a_{nn})/2 - a_{np}$, and of class III CSB interaction [39], but has not been studied for class IV forces. Further work on this contribution is needed before CSB in np scattering can be said to be understood. This need is even more compelling, if one considers the possibility that $\rho\omega$ mixing is strongly different for off-shell meson exchanges as compared with isospin violating on-shell decays or formation of ρ and ω mesons. Recently a simple quark model based calculation of Ref. [40] suggests that due to this effect the $\rho\omega$ mixing potential would be negligible in practice.

ACKNOWLEDGMENTS

I am grateful to S. E. Vigdor for producing the minimal variance results of Figs. 18 and 19. This work was partly supported by the Academy of Finland and NSF Grant No. PHY 90-15957. I acknowledge the hospitality of both IUCF and TRIUMF, where the work was started.

[1] E. M. Henley and G. A. Miller, in *Mesons and Nuclei,* edited by M. Rho and D. Wilkinson (North-Holland, Amsterdam, 1979), Vol. I, p. 416.
[2] R. Abegg *et al.*, Phys. Rev. Lett. **56**, 2571 (1986); Phys. Rev. D **39**, 2464 (1989).
[3] L. D. Knutson, S. E. Vigdor, W. W. Jacobs, J. Sowinski, P. L. Jolivette, S. W. Wissink, C. Bloch, C. Whiddon, and R. C. Byrd, Phys. Rev. Lett. **66**, 1410 (1991); S. E. Vigdor, W. W. Jacobs, L. D. Knutson, J. Sowinski, C. Bloch, P. L. Jolivette, S. W. Wissink, R. C. Byrd, and C. Whiddon, Phys. Rev. C (to be published).
[4] R. R. Tkachuk, L. G. Greeniaus, and W. T. H. van Oers, TRIUMF experiment 369 proposal; L. G. Greeniaus, in *Proceedings of the Symposium on Spin and Symmetries* [11].
[5] L. Ge and J. P. Svenne, Phys. Rev. C **33**, 417 (1986); **34**, 756(E) (1986).
[6] G. A. Miller, A. W. Thomas, and A. G. Williams, Phys. Rev. Lett. **56**, 2567 (1986); A. G. Williams, A. W. Thomas, and G. A. Miller, Phys. Rev. C **36**, 1956 (1987).
[7] R. Holzenkamp, K. Holinde, and A. W. Thomas, Phys. Lett. B **195**, 121 (1987).
[8] M. J. Iqbal and J. A. Niskanen, Phys. Rev. C **38**, 2259 (1988).
[9] M. Beyer and A. G. Williams, Phys. Rev. C **38**, 779 (1988); A. G. Williams, in *Proceedings of the Symposium on Spin and Symmetries* [11].
[10] M. J. Iqbal, J. Thaler, and R. M. Woloshyn, Phys. Rev. C **36**, 2442 (1987).
[11] *Proceedings of the Symposium on Spin and Symmetries,* TRIUMF, Vancouver, 1989, edited by W. D. Ramsay and W. T. H. van Oers (TRIUMF Report No. TRI-89-5).
[12] G. A. Miller, B. M. K. Nefkens, and I. Slaus, Phys. Rep. **144C**, 1 (1991).
[13] K. Bräuer, E. M. Henley, and G. A. Miller, Phys. Rev. C **34**, 1779 (1986).
[14] P. LaFrance and P. Winternitz, J. Phys. (Paris) **41**, 1391 (1980); J. Bystricky, F. Lehar, and P. Winternitz, *ibid.* **45**, 207 (1984).
[15] M. H. Partovi and E. L. Lomon, Phys. Rev. D **2**, 1999 (1970).
[16] S. A. Coon and M. D. Scadron, Phys. Rev. C **26**, 2402 (1983); T. E. O. Ericson and G. A. Miller, Phys. Lett. **132B**, 32 (1983).
[17] C. Y. Cheung and R. Machleidt, Phys. Rev. C **34**, 1181 (1986).
[18] J. R. Bergevoet, P. C. van Campen, R. A. M. Klomp, J.-L. de Kok, T. A. Rijken, V. G. J. Stoks, and J. J. de Swart, Phys. Rev. C **41**, 1435 (1990); R. A. Arndt, Z. Li, L. D. Roper, and R. L. Workman, Phys. Rev. Lett. **65**, 157 (1990); R. G. E. Timmermans, Th. A. Rijken, and J. J. de Swart, *ibid.* **67**, 1074 (1991); R. A. M. Klomp, V. G. J. Stoks, and J. J. de Swart, Phys. Rev. C **44**, 1258 (1991).
[19] R. V. Reid, Ann. Phys. (N.Y.) **50**, 411 (1968).
[20] J. A. Niskanen, M. Sebestyen, and A. W. Thomas, Phys. Rev. C **38**, 838 (1988).
[21] H. Sugawara and F. von Hippel, Phys. Rev. **172**, 1764 (1968).
[22] E. Pedroni *et al.*, Nucl. Phys. **A300**, 321 (1980).
[23] J. A. Niskanen and A. W. Thomas, Phys. Rev. C **37**, 1755 (1988).
[24] J. A. Niskanen and A. W. Thomas, Aust. J. Phys. **41**, 31 (1988).
[25] L. M. Nath, B. Etemadi, and J. D. Kimel, Phys. Rev. D **3**, 2153 (1971); H. T. Williams, Phys. Rev. C **31**, 2297 (1985).
[26] J. W. Durso, M. Saarela, G. E. Brown, and A. D. Jackson, Nucl. Phys. **A278**, 445 (1977).
[27] C. B. Dover and J. M. Richard, Phys. Rev. C **25**, 1953 (1982).
[28] A. M. Green and J. A. Niskanen, Nucl. Phys. **A271**, 503 (1976); A. M. Green, J. A. Niskanen, and M. E. Sainio, J. Phys. G **4**, 1055 (1978).
[29] S. A. Coon and M. D. Scadron, Phys. Rev. C **23**, 1150 (1981); J. A. Niskanen, Phys. Lett. **107B**, 344 (1981); A. W. Thomas and K. Holinde, Phys. Rev. Lett. **63**, 2025 (1989); K. Holinde and A. W. Thomas, Phys. Rev. C **42**, 1195 (1990).
[30] R. Machleidt, K. Holinde, and Ch. Elster, Phys. Rep. **149**, 1 (1987).
[31] J. A. Niskanen, Phys. Lett. **112B**, 17 (1982).
[32] R. A. Arndt, L. D. Roper, R. A. Bryan, R. B. Clark, and B. J. VerWest, Phys. Rev. D **28**, 97 (1983).
[33] J. A. Niskanen, Nucl. Phys. **A298**, 417 (1978); Phys. Lett. **141B**, 301 (1984).
[34] O. Dumbrajs, R. Koch, H. Pilkuhn, G. C. Oades, H. Behrens, J. J. de Swart, and P. Kroll, Nucl. Phys. **B216**, 277 (1983).
[35] S. E. Vigdor, private communication, 1992.
[36] L. D. Knutson, private communication.
[37] J. A. Niskanen and S. E. Vigdor, Phys. Rev. C **45**, 3021 (1992).
[38] S. A. Coon and J. A. Niskanen, in preparation.
[39] D. O. Riska and Y. H. Chu, Nucl. Phys. **A235**, 499 (1974).
[40] T. Goldman, J. A. Henderson, and A. W. Thomas, University of Adelaide Report ADP-91-158/T98.
[41] J. Stahov, M. E. Sadler, and V. V. Abaev, Phys. Rev. Lett. **68**, 548 (1992).